ENHANCED GENERATIVE MODEL EVALUATION WITH CLIPPED DENSITY AND COVERAGE

Anonymous authors
Paper under double-blind review

ABSTRACT

Although generative models have made remarkable progress in recent years, their use in critical applications has been hindered by an inability to reliably evaluate the quality of their generated samples. Quality refers to at least two complementary concepts: fidelity and coverage. Current quality metrics often lack reliable, interpretable values due to an absence of calibration or insufficient robustness to outliers. To address these shortcomings, we introduce two novel metrics: *Clipped Density* and *Clipped Coverage*. By clipping individual sample contributions, as well as the radii of nearest neighbor balls for fidelity, our metrics prevent out-of-distribution samples from biasing the aggregated values. Through analytical and empirical calibration, these metrics demonstrate linear score degradation as the proportion of bad samples increases. Thus, they can be straightforwardly interpreted as equivalent proportions of good samples. Extensive experiments on synthetic and real-world datasets demonstrate that *Clipped Density* and *Clipped Coverage* outperform existing methods in terms of robustness, sensitivity, and interpretability when evaluating generative models.

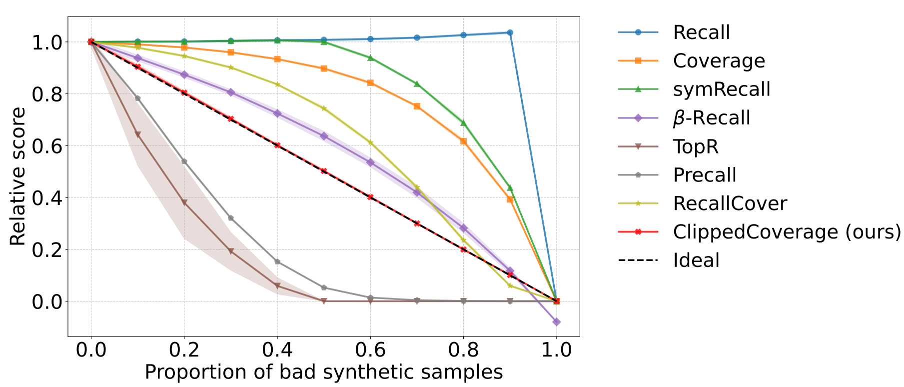

Figure 1: **Measuring the coverage of a mixture of good and bad samples (CIFAR-10)**: Various coverage metrics are evaluated relative to their maximum value as the proportion of bad synthetic samples increases. Only *Clipped Coverage* displays the desired linear degradation.

1 INTRODUCTION

In recent years, remarkable progress has been achieved in generative models, which are being actively explored in various fields, such as healthcare (Pinaya et al., 2022; Fernandez et al., 2024; Tudosiu et al., 2024; Zhu et al., 2024; Bluethgen et al., 2024). However, deploying them in high-stakes applications depends on reliably evaluating the quality of synthetic data to ensure its trustworthiness. This evaluation is inherently challenging, especially for high-dimensional data. The true underlying distributions of this data are often unknown and complex. They also do not conform to known parametric families. These factors make computing the support or density infeasible in practice. Current model evaluation often relies on metrics such as Fréchet Inception Distance (FID) (Heusel et al., 2017) and FD-DINOv2 (Stein et al., 2023) for images. These metrics provide a single, compound score representing overall sample quality. Thus, it is impossible to determine whether poor performance stems from a lack of realism or variety (Sajjadi et al., 2018).

To address this issue, the quality of synthetic data can be broken down into at least two core concepts: fidelity and coverage. Fidelity assesses how similar each synthetic sample is to the input data (Naeem et al., 2020). Conversely, coverage measures the extent to which synthetic samples represent the distribution of real data, taking into consideration how the rarity or commonness of real data is reflected in the synthetic samples. However, a recent position paper by Räisä et al. (2025) argues that all existing fidelity and diversity metrics are flawed, highlighting an urgent need for new metrics that address these shortcomings.

To determine whether generative models can be truly dependable, particularly in sensitive applications, the metrics used to evaluate them must be trustworthy. This means that they must be robust, sensitive to genuine deficiencies, and provide interpretable scores. A key challenge is robustness to outliers. Real-world datasets often contain out-of-distribution samples such as corruptions, anomalies, or simply samples very different from the rest (see Figure 7 for examples in CIFAR-10). Similarly, generative models can produce "bad" samples that are far from the real data distribution. These outliers can disproportionately influence evaluation scores, masking true performance issues.

Beyond robustness, interpretability is crucial. Metrics should offer more than just relative comparisons (i.e., knowing that one model is better than another). As emphasized by Räisä et al. (2025), for a metric to be truly useful in practice, its absolute value must be meaningful, since even the best-performing model in a comparison might still be of poor quality. Critically, Räisä et al. (2025) notes that, currently, no metric offers this property. Ideally, for straightforward interpretability, a score of x would indicate performance equivalent to having a proportion of x good samples and $(1-x)$ bad ones. However, as shown in Figure 1, current coverage metrics fail to achieve this. We show in Figure 4 that current fidelity metrics are similarly untrustworthy.

In this paper, we introduce *Clipped Density* and *Clipped Coverage*, two novel metrics designed to overcome these limitations. Our contributions are:

- **Trustworthy Evaluation**: Our metrics achieve robustness to outliers by clipping individual sample contributions to the aggregate score and, for *Clipped Density*, by limiting the radii of nearest-neighbor spheres used to measure the density. This prevents out-of-distribution samples from skewing the evaluation while preserving sensitivity to genuine issues.
- **Interpretable Absolute Scores**: Through empirical calibration for *Clipped Density* and theoretical analysis for *Clipped Coverage*, we ensure that scores degrade linearly with the proportion of bad samples, providing absolute interpretability.

The paper is structured as follows: Section 2 provides background on existing metrics. Section 3 reviews related work. Section 4 introduces our *Clipped Density* and *Clipped Coverage* metrics. Section 5 details our experiments and results, and Section 6 discusses implications and limitations.

2 Background

We consider a setting in which we are given N i.i.d. samples $\{x_i^r\}_{i=1}^N$ from an unknown data (reference, or real) distribution p_r and M i.i.d. samples $\{x_j^s\}_{j=1}^M$ generated from an unknown synthetic data distribution p_s. In this section, we review relevant metrics for evaluating generative models that aim to disentangle two aspects of synthetic data: fidelity (how realistic each synthetic sample is) and coverage (how well the synthetic samples populate the real density distribution). These metrics serve as the basis for our proposed improvements.

Assuming given supports S^r for the real distribution and S^s for the synthetic distribution, *Precision* measures the proportion of synthetic samples that fall within S^r, while *Recall* measures the proportion of i.i.d. real samples that fall in S^s (Sajjadi et al., 2018; Simon et al., 2019).

$$\text{Precision} = \mathbb{P}_{p_s}[S^r] = \mathbb{P}_{p_s}[S^r \cap S^s] \qquad \text{Recall} = \mathbb{P}_{p_r}[S^s] = \mathbb{P}_{p_r}[S^r \cap S^s] \tag{1}$$

However, the underlying densities d^r and d^s and their supports S^r and S^s are unknown, making such computation infeasible. In practice, *improved Precision* and *Recall* (Kynkäänniemi et al., 2019) approximate these supports by the union of balls centered at each observed sample, with a radius equal to the distance NND_k from its center to its k-th Nearest Neighbor (Burman & Nolan, 1992). We denote by NND_k^r and NND_k^s the distance to the k-th nearest real and synthetic sample, respectively.

$$\text{iPrecision} = \mathbb{P}_{p_s}[\hat{S}^r \cap S^s] = \frac{1}{M}\sum_{j=1}^{M} \mathbf{1}_{x_j^s \in \cup_{i=1}^{N} B(x_i^r, \mathrm{NND}_k^r(x_i^r))} \tag{2}$$

$$\text{iRecall} = \mathbb{P}_{p_r}[S^r \cap \hat{S}^s] = \frac{1}{N}\sum_{i=1}^{N} \mathbf{1}_{x_i^r \in \cup_{j=1}^{M} B(x_j^s, \mathrm{NND}_k^s(x_j^s))} \tag{3}$$

Yet, *iPrecision* and *iRecall* are strongly biased by out-of-distribution samples. Real outliers, being far from their nearest neighbors, create large balls and bias the estimation of S^r. Similarly, bad synthetic samples compromise the approximation of the synthetic support (Naeem et al., 2020).

Density and *Coverage* (Naeem et al., 2020) aim to alleviate this issue by going beyond a binary in/out decision. *Density* counts, for each synthetic sample, how many real k-NN balls it falls within, normalized by k. Thus, outliers with large balls contribute only $\frac{1}{k}$ to the fidelity of a given synthetic sample, instead of 1 for *iPrecision* (Naeem et al., 2020). In high-dimensional spaces, where measuring density is impractical, *Density* instead uses k-NN balls as a proxy. It represents the average relative density d^s/d^r, providing a relative measure of how many synthetic points fall within real balls, normalized by their mass k. To avoid estimation bias when approximating the synthetic distribution, which may contain many bad samples, additional considerations are needed. *Coverage* flips the perspective (Naeem et al., 2020): instead of computing the proportion of real samples within at least one synthetic ball, *Coverage* calculates the proportion of real samples that are *covered*, by having at least one synthetic sample within their ball: Coverage $= \mathbb{P}_{p_r}[\hat{S}^r \cap S^s]$.

$$\text{Density} = \frac{1}{kM}\sum_{j=1}^{M}\sum_{i=1}^{N} \mathbf{1}_{x_j^s \in B(x_i^r, \mathrm{NND}_k^r(x_i^r))} \qquad \text{Coverage} = \frac{1}{N}\sum_{i=1}^{N} \mathbf{1}_{\exists j, x_j^s \in B(x_i^r, \mathrm{NND}_k^r(x_i^r))} \tag{4}$$

Although *Density* is less affected by outliers in the target distribution, it remains influenced by them (Park & Kim, 2023). Additionally, *Density* is not bounded by 1 (Naeem et al., 2020), making interpretation challenging when empirical estimates exceed this value (Cheema & Urner, 2023; Kim et al., 2023). Similar to *iPrecision* and *iRecall*, *Coverage* is limited to analyzing supports and misses density mismatches: a few synthetic samples can cover high-density regions by lying within many real balls, and adding more synthetic samples there might not increase the score (Park & Kim, 2023).

3 Related Work

Recent works have aimed to improve these metrics. *Precision Cover* and *Recall Cover*, analogous to *Precision* and *Recall*, were introduced by Cheema & Urner (2023). They count a ball as covered only if it contains at least $k' > 1$ samples. A probabilistic approach was introduced by Park & Kim (2023): *P-precision* and *P-recall*. These measure the probability that a synthetic (resp., real) sample lies within a random sub-support of the real (resp., synthetic) distribution.

To address the problem of large-radius balls, Khayatkhoei & AbdAlmageed (2023) have employed a dual-perspective approach with *symPrecision* and *symRecall*: *symRecall* is defined as the minimum of *Recall* and *Coverage*, while *symPrecision* is the minimum of *Precision* and the *complementary Precision* metric computed from the reversed perspective. Some alternative approaches do not rely on nearest-neighbor approximations. *α-Precision* and *β-Recall* (Alaa et al., 2022) employ a one-class approach to estimate supports containing a fraction α (resp. β) of a dataset. They measure the proportion of the other dataset found within supports of varying levels. *Topological Precision and Recall* (Kim et al., 2023) estimate support via topologically conditioned density kernels.

Recently, Räisä et al. (2025) developed a benchmark of sanity checks for generative model metrics using synthetic data, finding that all existing fidelity and coverage metrics are flawed. Our own tests based on real-world data (Figures 1, 4 and 5) confirm this conclusion. That work further emphasizes that no current metric is suitable for absolute evaluations, calling for more research in this area. Our work addresses these concerns directly by introducing new metrics that overcome these limitations. We show in Appendix H that our proposed metrics also perform well on their synthetic benchmark.

In the following section, we introduce metrics designed to resolve these issues by being *i)* robust to outliers, and by *ii)* providing clearly interpretable values.

4 METHOD

Our proposed metrics are designed to satisfy several key properties. Firstly, they should be *robust to outliers* (Desideratum 1). Secondly, the metrics should exhibit *linear score degradation*: if a proportion x of samples are bad, the score should decrease by x (Desideratum 2a). The metrics should be *normalized* between 0 and 1 (Desideratum 2b), allowing their values to be interpreted on their own.

These properties enable straightforward interpretations: a score of x indicates that the synthetic dataset achieves the same fidelity or coverage as a dataset composed of a proportion x of real samples and $(1-x)$ bad samples. A difference of y between two datasets corresponds to y more bad samples in the equivalent scoring scenario.

4.1 CLIPPED DENSITY

4.1.1 A ROBUST FIDELITY METRIC

To measure fidelity, the *Density* metric counts the number of real balls each synthetic sample falls within. This approach can exceed 1 and is vulnerable to outliers, as it relies on adaptive ball radii.

Figure 2 illustrates a failure case of the *Density* metric on a synthetic dataset containing a single bad sample (bottom left), with $k = 2$. In this configuration, the two centered points each receive a fidelity score of $\frac{3}{2}$, while the bad sample obtains a fidelity of 0. So, the overall dataset fidelity is computed as $\frac{1}{3}\left(2 \times \frac{3}{2} + 0\right) = 1$: an ideal score. While this is an example in dimension 2, the problem worsens in higher dimensions as the number of balls a sample can belong to increases (Radovanovic et al., 2010), allowing one over-occurring sample to mask an increasing number of bad synthetic samples.

To prevent over-occurring samples from masking defects, we modify the aggregation approach. The intuitive idea is to limit the contribution of each sample to the metric: the fidelity of any synthetic sample should not exceed 1. Applying this modification to Figure 2, the fidelity score becomes $\frac{1}{3}\left(2 \times \min(\frac{3}{2}, 1) + 0\right) = \frac{2}{3}$, which effectively detects the presence of the bad sample.

On the other hand, real outliers can have extremely large distances to their nearest neighbors, resulting in balls with significantly larger radii. In dimension d, the volume of a ball of radius r is proportional to r^d. Not only do outliers create much larger balls, but any point in a low-density region does so as well, which dramatically skews the metrics. These balls have a fixed *mass* k, but their *volume* varies. Balls of large *volume* can contribute disproportionately more than the others. To ensure balanced contributions that limit outlier influence, we clip the radius of each ball to the median of the distances to the k-th nearest neighbor.

$$R_k(x_i^r) = \min\left(\mathrm{NND}_k^r(x_i^r), \mathrm{median}(\{\mathrm{NND}_k^r(x_l)\}_{l=1}^N)\right) \tag{5}$$

This results in the following metric that satisfies Desideratum 1, robustness to outliers:

$$\mathrm{ClippedDensity}_{\mathrm{unnorm}} = \frac{1}{M}\sum_{j=1}^{M}\min\left(\frac{1}{k}\underbrace{\sum_{i=1}^{N}\mathbf{1}_{x_j^s \in B(x_i^r, R_k(x_i^r))}}_{\#\{\text{clipped real balls } x_j^s \text{ is within}\}}, 1\right) \tag{6}$$

4.1.2 NORMALIZING FOR INTERPRETABILITY

Since $\mathrm{ClippedDensity}_{\mathrm{unnorm}}$ is an average over synthetic samples, a proportion x of bad samples directly reduces the score by x, satisfying Desideratum 2a. To achieve normalization between 0 and 1 (Desideratum 2b), we require an ideal value of 1. We achieve this ideal value empirically by evaluating the fidelity score of the real data using a leave-one-out strategy. For each sample x_i^r, we count the number of clipped real balls j (with $j \neq i$) that contain it. This computation is efficient, as we have already obtained the indices of real samples inside each ball during the radius computation.

We normalize $\mathrm{ClippedDensity}_{\mathrm{unnorm}}$ by the value computed for real data, $\mathrm{ClippedDensity}_{\mathrm{real}}$, and clip the result to 1, since scores exceeding 1 would lack meaningful interpretation. The final normalized metric is:

$$\mathrm{ClippedDensity} = \min\left(\frac{\mathrm{ClippedDensity}_{\mathrm{unnorm}}}{\mathrm{ClippedDensity}_{\mathrm{real}}}, 1\right) \tag{7}$$

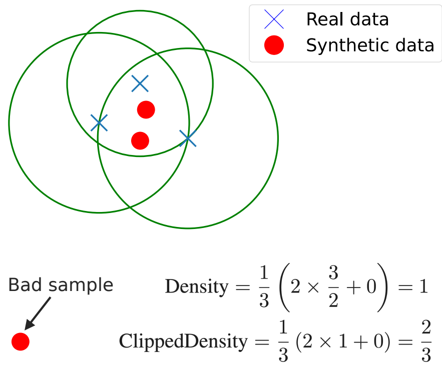

Figure 2: ***Clipped Density* corrects *Density*'s failure**: In a simple setup with a single bad synthetic sample, *Density* yields a value of 1. By clipping the fidelity of individual samples to 1, we obtain an adjusted score of $\frac{2}{3}$.

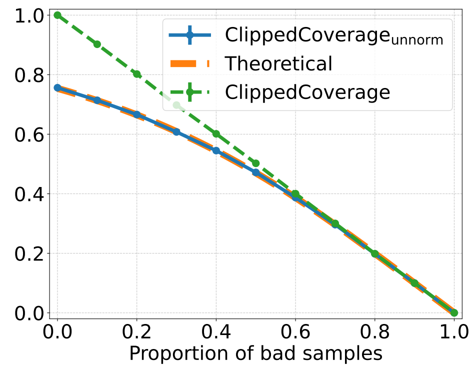

Figure 3: **Correcting *Clipped Coverage* linear decay**: The *unnormalized Clipped Coverage* (blue) does not decrease linearly with the proportion of bad samples. We theoretically compute its expected behavior (orange) and correct it (green).

4.2 Clipped Coverage

4.2.1 A Robust Coverage Metric

To measure coverage, the *Coverage* metric considers the proportion of real samples whose balls contain at least one synthetic sample. To reflect the real data *distribution* and not just its support, we adopt an approach similar to *Clipped Density*. Instead of only checking for the presence of synthetic samples inside a real ball, we count how many there are. Then, to bound the contribution of each real sample, individual coverage scores are capped at 1. This results in the following formulation:

$$\text{ClippedCoverage}_{\text{unnorm}} = \frac{1}{N}\sum_{i=1}^{N} \min\left(\frac{1}{k} \underbrace{\sum_{j=1}^{M} \mathbf{1}_{x_j^s \in B(x_i^r, \text{NND}_k^r(x_i^r))}}_{\#\{\text{synthetic samples within } x_i^r\text{'s ball}\}}, 1\right) \tag{8}$$

For each real sample, we compare the *mass* of synthetic samples in its ball to the *mass* of real samples. To balance real points' contributions, the *mass* of each ball is fixed: no radius clipping is applied. $\text{ClippedCoverage}_{\text{unnorm}}$ satisfies Desideratum 1 of robustness to outliers.

4.2.2 Calibrating for Interpretability

The blue curve in Figure 3 shows $\text{ClippedCoverage}_{\text{unnorm}}$ when the real and synthetic distributions are identical (far left) and as bad samples are progressively introduced into the synthetic distribution. To satisfy Desideratum 2, the score should follow $1 - x$ for x, the proportion of bad samples. To correct the metric's behavior, we start by deriving its expected value as a function of x.

Lemma 1. *If the real and synthetic distributions are identical, i.e., $\{x_i^r\}_{i=1}^N$ and $\{x_j^s\}_{j=1}^M$ are $N+M$ i.i.d. samples from the same distribution, then the expected value of $\mathit{ClippedCoverage}_{\mathit{unnorm}}$ is:*

$$\mathbf{E}\left[\mathit{ClippedCoverage}_{\mathit{unnorm}}\right] = \sum_{j=1}^{M} \min\left(\frac{j}{k}, 1\right)\binom{M}{j}\frac{\beta(k+j, M-j+N-k)}{\beta(k, N-k)} \tag{9}$$

where β is the beta function.

The proof of Lemma 1 is provided in Appendix A. To parameterize the curve, we now consider the case with a proportion x of bad synthetic samples. Since such samples always lie outside any real ball, the expected score becomes equivalent to the ideal case in Lemma 1 but with $M_x = \lfloor M(1-x) \rfloor$ synthetic samples instead of M. We denote this as $f_{\text{expected}}(x)$, shown in orange in Figure 3.

To satisfy Desideratum 2, the expected value of the metric should be $1 - x$ when the proportion of bad samples is x. This calibration ensures both a linear degradation of the score (Desideratum 2a) and normalization to a consistent [0, 1] range regardless of the dataset or choice of k (Desideratum 2b). We seek a function g such that $g \circ f_{\text{expected}}(x) = 1 - x$. Since M_x can only take integers values m between 0 and M, it suffices to find g for $f_{\text{expected}}(M_x = m)$ where $m \in \{0, \ldots, M\}$.

We can efficiently compute $f_{\text{expected}}(M_x = m)$ for all m (see Appendix B.1). Given these values, the function g is computed numerically. Since f_{expected} decreases with x, we reverse it to form a sorted list of f_{expected} values. For a given $\text{ClippedCoverage}_{\text{unnorm}}$ score s, we find the index $i(s) \in \{0, \ldots, M\}$ such that inserting the value s at index $i(s)$ keeps the list sorted. Then, $g(s) = 1 - \frac{i(s)}{M}$. The final normalized metric, which recovers the desired behavior shown in green in Figure 3, is:

$$\text{ClippedCoverage} = g \circ \text{ClippedCoverage}_{\text{unnorm}} \tag{10}$$

5 Experiments

5.1 Experimental Setup

We compared our metrics against multiple baselines, using the original code for *α-Precision*, *β-Recall*, and *TopP&R*, and reimplementing *Precision*, *Recall*, *Density*, *Coverage*, *symPrecision*, *symRecall*, *P-precision*, *P-recall*, and *Precision Recall Cover* for performance reasons (see Appendix B.2 for comparisons). For consistency, we set $k = 5$ where applicable; $k' = 3$ and $C = 3$, as recommended for *Precision Recall Cover*, and used default parameters everywhere else.

Experiments were conducted on a single NVIDIA H100 GPU with 80GB of RAM. When images are evaluated, metrics are computed on image data in the embedding space of the "Large" DINOv2 model (DINOv2-ViT-L/14 (Oquab et al., 2023)), as recommended by Stein et al. (2023).

5.2 Metric Evaluation Tests

To ensure proper behavior, we evaluated metrics in various scenarios by controlling dataset composition and hence the expected scores. Most tests were performed on CIFAR-10 (Krizhevsky et al., 2009), with 2500 samples from each of the 10 classes for the real set and the other 2500 for the synthetic set. We report mean ± std over 10 splits. Results are summarized in Figures 4e and 5c.

CIFAR-10 Simultaneous mode dropping: To verify that fidelity metrics do not capture coverage, we performed a simultaneous mode dropping test on CIFAR-10 (Figure 4b, from Naeem et al. (2020)). In this test, the synthetic set progressively replaced samples from all but one class with samples from the remaining class, while the real set remained unchanged. Since the synthetic set is always a subset of CIFAR-10, fidelity scores should remain stable and close to their maximum. However, *Precision Cover* (yellow) and *symPrecision* (green) appear to capture coverage, as they deviate from their maximum value, while *α-Precision* (purple) shows high instability (high std).

CIFAR-10 matched real and synthetic out-of-distribution sample proportion: To evaluate robustness to out-of-distribution samples, we conducted a test on CIFAR-10 (Figures 4c and 5a, inspired by Figure 5 of Naeem et al. (2020)), where we progressively replaced both real and synthetic CIFAR-10 samples with out-of-distribution samples (noise images) at the same rate. Since the synthetic set is constructed identically to the real set in all cases, scores should remain stable and close to their maximum value. However, *α-Precision* and *β-Recall* (purple), *TopP* and *TopR* (brown), and *P-precision* and *P-Recall* (gray) show instability and deviate from the expected value.

Synthetic data translation: Since real-world datasets like CIFAR-10 contain outliers, we use a test based on synthetic data (Figures 4d and 5b, adapted from Naeem et al. (2020)) to evaluate robustness to the first out-of-distribution sample. We use 25000 standard Gaussian samples (dim 32, 5 splits). The synthetic set is translated by $\mu \in [-\mathbf{1}, \mathbf{1}]$ in all dimensions and includes a bad sample at $-\mathbf{3}$. The real set includes an outlier at $\mathbf{3}$. Ideally, scores should form symmetric bell-shaped curves, dropping rapidly as μ moves away from 0 to detect distribution shifts. For fidelity (Figure 4d), *Precision* (blue) and *Density* (orange) are non-symmetric due to the real outlier's large ball, which in turn affects *symPrecision* (green). *α-Precision* (purple) and *P-precision* (gray) show low sensitivity (flat curves around 0). For coverage (Figure 5b), *Recall* (blue) is non-symmetric due to the bad synthetic sample, which also affects *symRecall* (green). This happens because the bad sample's ball grows as the rest of the synthetic data moves away, covering the real set when μ is near $\mathbf{1}$. *β-recall* (purple) and *TopR* (brown) are also non-symmetric, indicating instability or insufficient robustness.

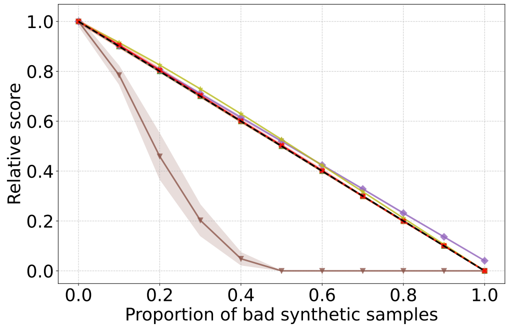

(a) Fidelity reduction with bad samples (CIFAR-10)

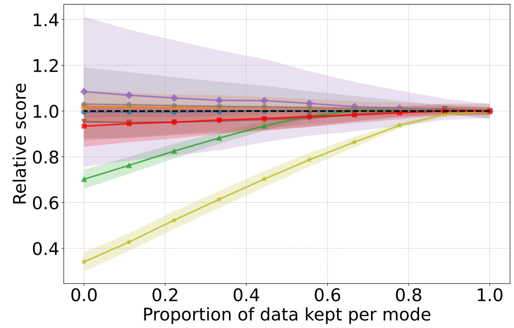

(b) Simultaneously dropping modes (CIFAR-10)

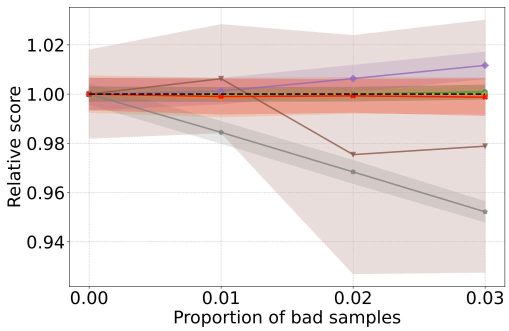

(c) Introducing bad real & syn. samples (CIFAR-10)

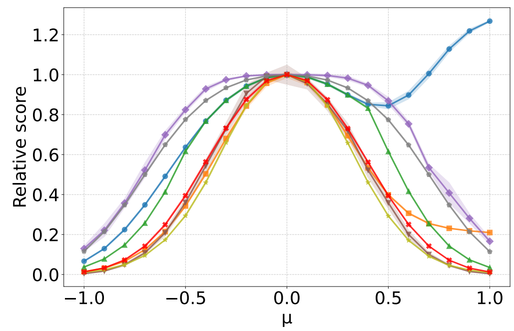

(d) Translating syn. Gaussian with 2 bad samples

Legend	Figure 4a	Figure 4b	Figure 4c	Figure 4d
Precision	✓	✓	✓	✗
Density	✓	✓	✓	✗
symPrecision	✓	✗	✓	✗
α-Precision	✓	✗	✗	✗
TopP	✗	✓	✗	✓
Pprecision	✓	✓	✗	✗
PrecisionCover	✓	✗	✓	✓
ClippedDensity (ours)	✓	✓	✓	✓
Ideal				

(e) Legend and summary

Figure 4: **Testing fidelity metrics** (legend/summary in (e)). Scenarios: (a) increasing bad synthetic sample proportion; (b) simultaneous mode dropping: progressively replacing all but one class with the last class; (c) matched real & synthetic out-of-distribution samples at equal rates; (d) synthetic distribution translation with one real outlier and one bad synthetic sample. Only *Clipped Density* consistently behaves as expected: linearity (a), stability (b, c), and symmetry with sensitivity (d).

CIFAR-10 Progressive bad sample introduction: To test sensitivity and interpretability, we progressively introduced bad samples (noise images) into a synthetic set of CIFAR-10 images (Figures 1 and 4a). Scores should decrease linearly with the proportion of bad samples (see Section 4). For coverage metrics, only *Clipped Coverage* (red) exhibited this linear degradation. Most fidelity metrics, being averages of individual sample fidelities, decreased linearly. However, *TopP* (brown) deviated significantly, while *Precision Cover* (yellow) and α*-Precision* (purple) showed slight deviations.

Summary: Across all results (see also Figures 4e and 5c), only *Clipped Density* and *Clipped Coverage* show the desired behavior in all tests. Other fidelity metrics either inappropriately capture coverage (e.g., *symPrecision,* α*-Precision, Precision Cover*), lack sensitivity (e.g., *P-precision*), or lack robustness to outliers (e.g., *Precision, Density, TopP*). For coverage metrics, only *Clipped Coverage* shows a linear decrease in score with increasing bad sample fraction, while some metrics are also insufficiently robust to outliers (e.g., *Recall, symRecall,* β*-recall, TopR, P-recall*).

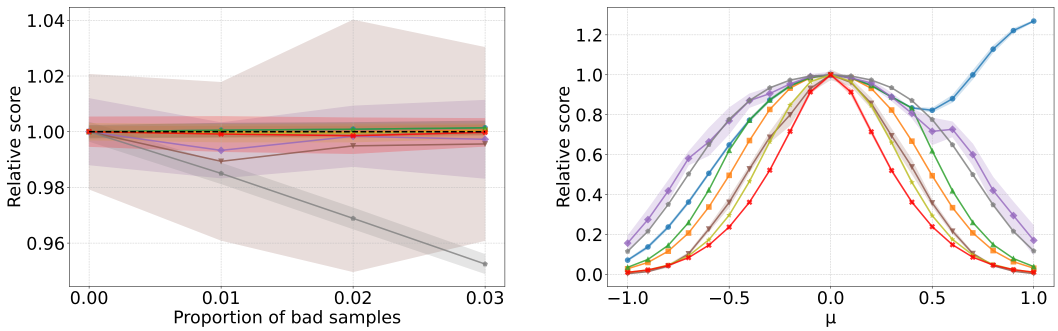

(a) Introducing bad real & syn. samples (CIFAR-10)   (b) Translating syn. Gaussian with 2 bad samples

Legend	Figure 1	Figure 5a	Figure 5b
Recall	✗	✓	✗
Coverage	✗	✓	✓
symRecall	✗	✓	✗
β-Recall	✗	✗	✗
TopR	✗	✗	✓
Precall	✗	✗	✗
RecallCover	✗	✓	✓
ClippedCoverage (ours)	✓	✓	✓
Ideal			

(c) Legend and summary

Figure 5: **Testing coverage metrics** (legend/result summary in (c)). Metrics are evaluated under different scenarios: (a) matched real & synthetic out-of-distribution samples; (b) distribution translation with a real outlier at **3** and a bad synthetic sample at **-3**. *Clipped Coverage* exhibits all desired properties: linearity (Figure 1), stability (a), symmetry and sensitivity (b), unlike other metrics.

5.3 Evaluation on Real Datasets

We evaluated various generative models on CIFAR-10 (Krizhevsky et al., 2009), ImageNet (Deng et al., 2009), LSUN Bedroom (Yu et al., 2015), and FFHQ (Kazemi & Sullivan, 2014) using categories and 50000 samples from the data publicly shared by Stein et al. (2023) (Figure 6 and appendix I). When possible, for conditional models, we kept an equal number of samples from each class (see Appendix C or Appendix A of Stein et al. (2023) for more details).

As shown in Figure 6, on CIFAR-10 and ImageNet, the *Density* values exceed 1, while the *Clipped Density* values remain stable. In Appendix D, we analyze RESFLOW-generated CIFAR-10 data, demonstrating that its inflated *Density* score of 2.47 results from real out-of-distribution samples. Additionally, Appendix E provides a detailed evaluation of *Clipped Density* on the generated datasets, quantifying the effect of each modification to the original *Density* metric.

Across all datasets, our results consistently show diffusion models outperforming GANs. The range of values that our metrics take seems to reflect the size of the training dataset: CIFAR-10 (50k samples, max score ≈ 0.4), FFHQ (70k, max ≈ 0.4), LSUN Bedroom (1.5M, max ≈ 0.7), and ImageNet (14M, max 1.0). Interpreting the absolute scores, a value of 0.4 for CIFAR-10 and FFHQ suggests that, on these datasets, top generative models achieve results equivalent to only 40% of good samples and 60% bad samples. This highlights substantial room for improvement, an insight only possible because the absolute values of *Clipped Density* and *Clipped Coverage* are interpretable.

6 Discussion and Conclusion

Clipped Density and *Clipped Coverage* offer significant improvements in robustness, sensitivity, and interpretability. To enhance robustness, we cap individual sample contributions at 1. For *Clipped Density*, we further mitigate outlier impact by clipping the *volumes* of real nearest-neighbor balls to

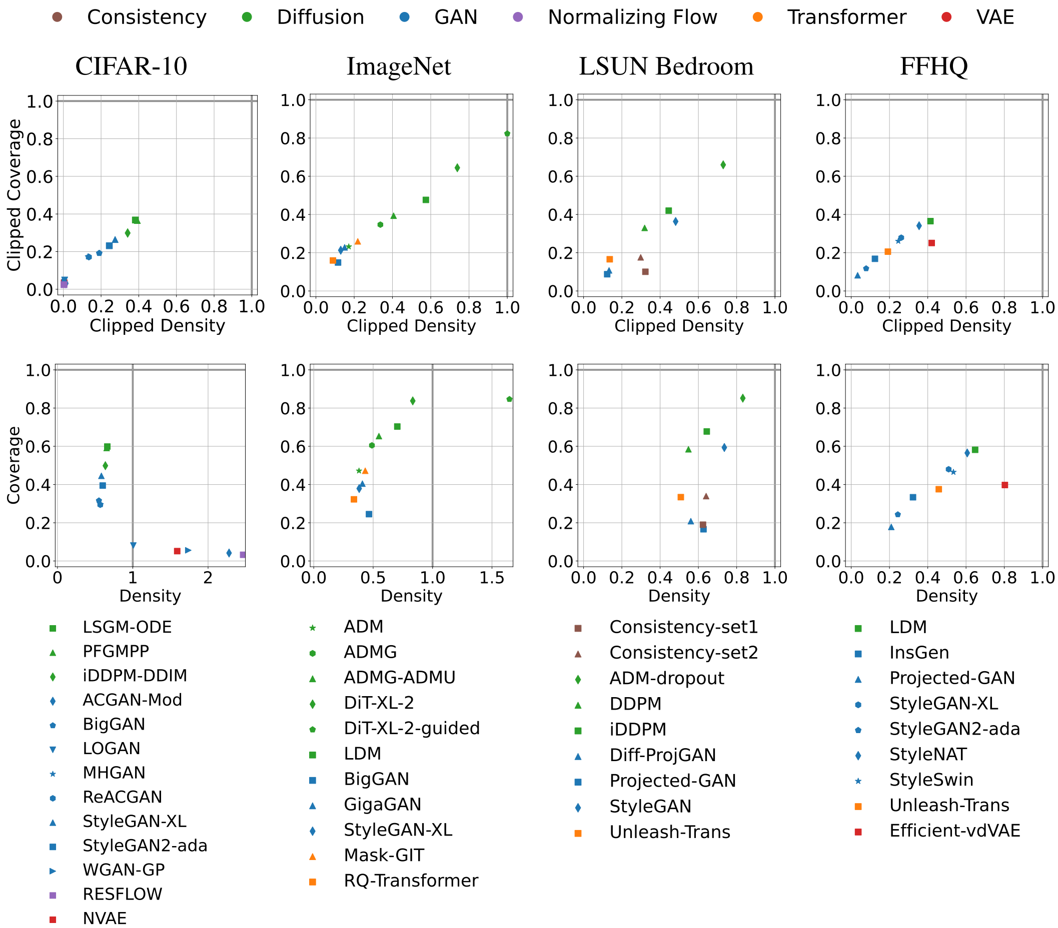

Figure 6: **Fidelity vs Coverage on various datasets**

prevent them from dominating the score. In contrast, for *Clipped Coverage*, we maintain balls of constant *mass* to ensure balanced contributions. Capping the contribution prevents high-performing samples from disproportionately hiding low-performing ones. This careful handling of sample contributions and ball properties enhances robustness while preserving sensitivity.

For interpretability, both metrics are calibrated to degrade linearly as the proportion of bad samples increases. *Clipped Density* achieves this through normalization by the real data's score. For *Clipped Coverage*, whose uncalibrated behavior is non-linear (as shown in Figure 3), we theoretically derived its expected behavior and applied a correction to ensure linearity. This combination of robust aggregation and principled calibration allows *Clipped Density* and *Clipped Coverage* to provide not only trustworthy relative comparisons between models but also meaningful absolute scores. This is crucial in practice for assessing whether a model meets a required quality threshold.

Despite these improvements, limitations remain. *Clipped Density* and *Clipped Coverage* build on an accepted benchmark of progressively passed tests, but it is not exhaustive, and there might be missing cases. Additionally, while we evaluate fidelity and coverage, other aspects matter, such as *memorization*: are generated samples reproductions of training data? Memorization metrics include GAN-test (Shmelkov et al., 2018), identifiability (Yoon et al., 2020), authenticity (Alaa et al., 2022), and the calibrated l_2 distance (Carlini et al., 2023). We used DINOv2 as recommended (Stein et al., 2023), but comparing embedding models for generative model evaluation remains an open question.

In conclusion, *Clipped Density* and *Clipped Coverage* provide a trustworthy framework for generative model evaluation, offering robust, sensitive, and interpretable assessments. [1]

[1] Code: `https://anonymous.4open.science/r/ClippedDensityCoverage-EF8E`.

References

Ahmed Alaa, Boris Van Breugel, Evgeny S Saveliev, and Mihaela van der Schaar. How faithful is your synthetic data? sample-level metrics for evaluating and auditing generative models. In *International Conference on Machine Learning*, pp. 290–306. PMLR, 2022.

Christian Bluethgen, Pierre Chambon, Jean-Benoit Delbrouck, Rogier van der Sluijs, Małgorzata Połacin, Juan Manuel Zambrano Chaves, Tanishq Mathew Abraham, Shivanshu Purohit, Curtis P Langlotz, and Akshay S Chaudhari. A vision–language foundation model for the generation of realistic chest x-ray images. *Nature Biomedical Engineering*, pp. 1–13, 2024.

Sam Bond-Taylor, Peter Hessey, Hiroshi Sasaki, Toby P Breckon, and Chris G Willcocks. Unleashing transformers: Parallel token prediction with discrete absorbing diffusion for fast high-resolution image generation from vector-quantized codes. In *European Conference on Computer Vision*, pp. 170–188. Springer, 2022.

Andrew Brock, Jeff Donahue, and Karen Simonyan. Large scale gan training for high fidelity natural image synthesis. In *7th International Conference on Learning Representations, ICLR 2019, New Orleans, LA, USA, May 6-9, 2019*, 2019.

P Burman and D Nolan. Location-adaptive density estimation and nearest-neighbor distance. *Journal of Multivariate Analysis*, 40(1):132–157, 1992.

Nicolas Carlini, Jamie Hayes, Milad Nasr, Matthew Jagielski, Vikash Sehwag, Florian Tramer, Borja Balle, Daphne Ippolito, and Eric Wallace. Extracting training data from diffusion models. In *32nd USENIX Security Symposium (USENIX Security 23)*, pp. 5253–5270, 2023.

Huiwen Chang, Han Zhang, Lu Jiang, Ce Liu, and William T Freeman. Maskgit: Masked generative image transformer. In *Proceedings of the IEEE/CVF conference on computer vision and pattern recognition*, pp. 11315–11325, 2022.

Fasil Cheema and Ruth Urner. Precision recall cover: A method for assessing generative models. In *International Conference on Artificial Intelligence and Statistics*, pp. 6571–6594. PMLR, 2023.

Ricky TQ Chen, Jens Behrmann, David K Duvenaud, and Jörn-Henrik Jacobsen. Residual flows for invertible generative modeling. *Advances in Neural Information Processing Systems*, 32, 2019.

Jia Deng, Wei Dong, Richard Socher, Li-Jia Li, Kai Li, and Li Fei-Fei. Imagenet: A large-scale hierarchical image database. In *2009 IEEE conference on computer vision and pattern recognition*, pp. 248–255. Ieee, 2009.

Prafulla Dhariwal and Alexander Nichol. Diffusion models beat gans on image synthesis. *Advances in neural information processing systems*, 34:8780–8794, 2021.

Paul Embrechts and Marius Hofert. A note on generalized inverses. *Mathematical Methods of Operations Research*, 77:423–432, 2013.

Virginia Fernandez, Walter Hugo Lopez Pinaya, Pedro Borges, Mark S Graham, Petru-Daniel Tudosiu, Tom Vercauteren, and M Jorge Cardoso. Generating multi-pathological and multi-modal images and labels for brain mri. *Medical Image Analysis*, pp. 103278, 2024.

James E Gentle. *Computational statistics*, volume 308. Springer, 2009.

Ishaan Gulrajani, Faruk Ahmed, Martin Arjovsky, Vincent Dumoulin, and Aaron C Courville. Improved training of wasserstein gans. *Advances in neural information processing systems*, 30, 2017.

Louay Hazami, Rayhane Mama, and Ragavan Thurairatnam. Efficient-vdvae: Less is more. *arXiv preprint arXiv:2203.13751*, 2022.

Martin Heusel, Hubert Ramsauer, Thomas Unterthiner, Bernhard Nessler, and Sepp Hochreiter. Gans trained by a two time-scale update rule converge to a local nash equilibrium. *Advances in neural information processing systems*, 30, 2017.

Jonathan Ho, Ajay Jain, and Pieter Abbeel. Denoising diffusion probabilistic models. *Advances in neural information processing systems*, 33:6840–6851, 2020.

Qiang Huang and Anthony KH Tung. Lightweight-yet-efficient: Revitalizing ball-tree for point-to-hyperplane nearest neighbor search. In *2023 IEEE 39th International Conference on Data Engineering (ICDE)*, pp. 436–449. IEEE, 2023.

Marco Jiralerspong, Joey Bose, Ian Gemp, Chongli Qin, Yoram Bachrach, and Gauthier Gidel. Feature likelihood divergence: evaluating the generalization of generative models using samples. *Advances in Neural Information Processing Systems*, 36:33095–33119, 2023.

Minguk Kang, Woohyeon Shim, Minsu Cho, and Jaesik Park. Rebooting acgan: Auxiliary classifier gans with stable training. *Advances in neural information processing systems*, 34:23505–23518, 2021.

Minguk Kang, Joonghyuk Shin, and Jaesik Park. Studiogan: a taxonomy and benchmark of gans for image synthesis. *IEEE Transactions on Pattern Analysis and Machine Intelligence*, 45(12): 15725–15742, 2023a.

Minguk Kang, Jun-Yan Zhu, Richard Zhang, Jaesik Park, Eli Shechtman, Sylvain Paris, and Taesung Park. Scaling up gans for text-to-image synthesis. In *Proceedings of the IEEE/CVF conference on computer vision and pattern recognition*, pp. 10124–10134, 2023b.

Tero Karras, Timo Aila, Samuli Laine, and Jaakko Lehtinen. Progressive growing of gans for improved quality, stability, and variation. In *6th International Conference on Learning Representations, ICLR 2018, Vancouver, BC, Canada, April 30 - May 3, 2018, Conference Track Proceedings*. OpenReview.net, 2018.

Tero Karras, Samuli Laine, and Timo Aila. A style-based generator architecture for generative adversarial networks. In *Proceedings of the IEEE/CVF conference on computer vision and pattern recognition*, pp. 4401–4410, 2019.

Tero Karras, Miika Aittala, Janne Hellsten, Samuli Laine, Jaakko Lehtinen, and Timo Aila. Training generative adversarial networks with limited data. *Advances in neural information processing systems*, 33:12104–12114, 2020.

Vahid Kazemi and Josephine Sullivan. One millisecond face alignment with an ensemble of regression trees. In *Proceedings of the IEEE conference on computer vision and pattern recognition*, pp. 1867–1874, 2014.

Mahyar Khayatkhoei and Wael AbdAlmageed. Emergent asymmetry of precision and recall for measuring fidelity and diversity of generative models in high dimensions. In *International Conference on Machine Learning*, pp. 16326–16343. PMLR, 2023.

Pum Jun Kim, Yoojin Jang, Jisu Kim, and Jaejun Yoo. Topp&r: Robust support estimation approach for evaluating fidelity and diversity in generative models. *Advances in Neural Information Processing Systems*, 36:7831–7866, 2023.

Alex Krizhevsky, Geoffrey Hinton, et al. Learning multiple layers of features from tiny images. 2009.

Tuomas Kynkäänniemi, Tero Karras, Samuli Laine, Jaakko Lehtinen, and Timo Aila. Improved precision and recall metric for assessing generative models. *Advances in neural information processing systems*, 32, 2019.

Doyup Lee, Chiheon Kim, Saehoon Kim, Minsu Cho, and Wook-Shin Han. Autoregressive image generation using residual quantization. In *Proceedings of the IEEE/CVF Conference on Computer Vision and Pattern Recognition*, pp. 11523–11532, 2022.

Ting Liu, Andrew W Moore, Alexander Gray, and Claire Cardie. New algorithms for efficient high-dimensional nonparametric classification. *Journal of machine learning research*, 7(6), 2006.

Muhammad Ferjad Naeem, Seong Joon Oh, Youngjung Uh, Yunjey Choi, and Jaejun Yoo. Reliable fidelity and diversity metrics for generative models. In *International Conference on Machine Learning*, pp. 7176–7185. PMLR, 2020.

Alexander Quinn Nichol and Prafulla Dhariwal. Improved denoising diffusion probabilistic models. In *International conference on machine learning*, pp. 8162–8171. PMLR, 2021.

Augustus Odena, Christopher Olah, and Jonathon Shlens. Conditional image synthesis with auxiliary classifier gans. In *International conference on machine learning*, pp. 2642–2651. PMLR, 2017.

Stephen M Omohundro. Five balltree construction algorithms. 1989.

Maxime Oquab, Timothée Darcet, Théo Moutakanni, Huy Vo, Marc Szafraniec, Vasil Khalidov, Pierre Fernandez, Daniel Haziza, Francisco Massa, Alaaeldin El-Nouby, et al. Dinov2: Learning robust visual features without supervision. *arXiv preprint arXiv:2304.07193*, 2023.

Richard Osuala, Grzegorz Skorupko, Noussair Lazrak, Lidia Garrucho, Eloy García, Smriti Joshi, Socayna Jouide, Michael Rutherford, Fred Prior, Kaisar Kushibar, et al. medigan: a python library of pretrained generative models for medical image synthesis. *Journal of Medical Imaging*, 10(6): 061403–061403, 2023.

Dogyun Park and Suhyun Kim. Probabilistic precision and recall towards reliable evaluation of generative models. In *Proceedings of the IEEE/CVF international conference on computer vision*, pp. 20099–20109, 2023.

Fabian Pedregosa, Gaël Varoquaux, Alexandre Gramfort, Vincent Michel, Bertrand Thirion, Olivier Grisel, Mathieu Blondel, Peter Prettenhofer, Ron Weiss, Vincent Dubourg, et al. Scikit-learn: Machine learning in python. *the Journal of machine Learning research*, 12:2825–2830, 2011.

William Peebles and Saining Xie. Scalable diffusion models with transformers. In *Proceedings of the IEEE/CVF international conference on computer vision*, pp. 4195–4205, 2023.

Walter HL Pinaya, Petru-Daniel Tudosiu, Jessica Dafflon, Pedro F Da Costa, Virginia Fernandez, Parashkev Nachev, Sebastien Ourselin, and M Jorge Cardoso. Brain imaging generation with latent diffusion models. In *MICCAI Workshop on Deep Generative Models*, pp. 117–126. Springer, 2022.

Milos Radovanovic, Alexandros Nanopoulos, and Mirjana Ivanovic. Hubs in space: Popular nearest neighbors in high-dimensional data. *Journal of Machine Learning Research*, 11(sept):2487–2531, 2010.

Ossi Räisä, Boris van Breugel, and Mihaela van der Schaar. Position: All current generative fidelity and diversity metrics are flawed. In *Forty-second International Conference on Machine Learning Position Paper Track*, 2025.

Robin Rombach, Andreas Blattmann, Dominik Lorenz, Patrick Esser, and Björn Ommer. High-resolution image synthesis with latent diffusion models. In *Proceedings of the IEEE/CVF conference on computer vision and pattern recognition*, pp. 10684–10695, 2022.

Mehdi SM Sajjadi, Olivier Bachem, Mario Lucic, Olivier Bousquet, and Sylvain Gelly. Assessing generative models via precision and recall. *Advances in neural information processing systems*, 31, 2018.

Axel Sauer, Kashyap Chitta, Jens Müller, and Andreas Geiger. Projected gans converge faster. *Advances in Neural Information Processing Systems*, 34:17480–17492, 2021.

Axel Sauer, Katja Schwarz, and Andreas Geiger. Stylegan-xl: Scaling stylegan to large diverse datasets. In *ACM SIGGRAPH 2022 conference proceedings*, pp. 1–10, 2022.

Bradley Segal, David M Rubin, Grace Rubin, and Adam Pantanowitz. Evaluating the clinical realism of synthetic chest x-rays generated using progressively growing gans. *SN Computer Science*, 2 (4):321, 2021.

Konstantin Shmelkov, Cordelia Schmid, and Karteek Alahari. How good is my gan? In *Proceedings of the European conference on computer vision (ECCV)*, pp. 213–229, 2018.

Loïc Simon, Ryan Webster, and Julien Rabin. Revisiting precision and recall definition for generative model evaluation. *arXiv preprint arXiv:1905.05441*, 2019.

Yang Song, Prafulla Dhariwal, Mark Chen, and Ilya Sutskever. Consistency models. *International Conference on Machine Learning*, 2023.

George Stein, Jesse Cresswell, Rasa Hosseinzadeh, Yi Sui, Brendan Ross, Valentin Villecroze, Zhaoyan Liu, Anthony L Caterini, Eric Taylor, and Gabriel Loaiza-Ganem. Exposing flaws of generative model evaluation metrics and their unfair treatment of diffusion models. *Advances in Neural Information Processing Systems*, 36, 2023.

Petru-Daniel Tudosiu, Walter HL Pinaya, Pedro Ferreira Da Costa, Jessica Dafflon, Ashay Patel, Pedro Borges, Virginia Fernandez, Mark S Graham, Robert J Gray, Parashkev Nachev, et al. Realistic morphology-preserving generative modelling of the brain. *Nature Machine Intelligence*, pp. 1–9, 2024.

Ryan Turner, Jane Hung, Eric Frank, Yunus Saatchi, and Jason Yosinski. Metropolis-hastings generative adversarial networks. In *International Conference on Machine Learning*, pp. 6345–6353. PMLR, 2019.

Arash Vahdat and Jan Kautz. Nvae: A deep hierarchical variational autoencoder. *Advances in neural information processing systems*, 33:19667–19679, 2020.

Arash Vahdat, Karsten Kreis, and Jan Kautz. Score-based generative modeling in latent space. *Advances in neural information processing systems*, 34:11287–11302, 2021.

Steven Walton, Ali Hassani, Xingqian Xu, Zhangyang Wang, and Humphrey Shi. Stylenat: Giving each head a new perspective. *arXiv preprint arXiv:2211.05770*, 2022.

Xiaosong Wang, Yifan Peng, Le Lu, Zhiyong Lu, Mohammadhadi Bagheri, and Ronald M Summers. Chestx-ray8: Hospital-scale chest x-ray database and benchmarks on weakly-supervised classification and localization of common thorax diseases. In *Proceedings of the IEEE conference on computer vision and pattern recognition*, pp. 2097–2106. CVPR, 2017.

Zhendong Wang, Huangjie Zheng, Pengcheng He, Weizhu Chen, and Mingyuan Zhou. Diffusion-gan: Training gans with diffusion. In *The Eleventh International Conference on Learning Representations, ICLR 2023, Kigali, Rwanda, May 1-5, 2023*, 2023.

Yan Wu, Jeff Donahue, David Balduzzi, Karen Simonyan, and Timothy Lillicrap. Logan: Latent optimisation for generative adversarial networks. *arXiv preprint arXiv:1912.00953*, 2019.

Yilun Xu, Ziming Liu, Yonglong Tian, Shangyuan Tong, Max Tegmark, and Tommi Jaakkola. Pfgm++: Unlocking the potential of physics-inspired generative models. In *International Conference on Machine Learning*, pp. 38566–38591. PMLR, 2023.

Ceyuan Yang, Yujun Shen, Yinghao Xu, and Bolei Zhou. Data-efficient instance generation from instance discrimination. *Advances in Neural Information Processing Systems*, 34:9378–9390, 2021.

Jinsung Yoon, Lydia N Drumright, and Mihaela Van Der Schaar. Anonymization through data synthesis using generative adversarial networks (ads-gan). *IEEE journal of biomedical and health informatics*, 24(8):2378–2388, 2020.

Fisher Yu, Ari Seff, Yinda Zhang, Shuran Song, Thomas Funkhouser, and Jianxiong Xiao. Lsun: Construction of a large-scale image dataset using deep learning with humans in the loop. *arXiv preprint arXiv:1506.03365*, 2015.

Bowen Zhang, Shuyang Gu, Bo Zhang, Jianmin Bao, Dong Chen, Fang Wen, Yong Wang, and Baining Guo. Styleswin: Transformer-based gan for high-resolution image generation. In *Proceedings of the IEEE/CVF conference on computer vision and pattern recognition*, pp. 11304–11314, 2022.

Xi Zhu, Wei Zhang, Yijie Li, Lauren J O'Donnell, and Fan Zhang. When diffusion mri meets diffusion model: A novel deep generative model for diffusion mri generation. In *International Conference on Medical Image Computing and Computer-Assisted Intervention*, pp. 530–540. Springer, 2024.

CONTENTS

A PROOF OF LEMMA 1

Proof.

$$\begin{aligned}
\mathbb{E}\left[\frac{1}{N}\sum_{i=1}^{N}\min\left(\frac{1}{k}\sum_{j=1}^{M}\mathbf{1}_{x_j^s \in B(x_i^r, \mathrm{NND}_k^r(x_i^r))}, 1\right)\right] &= \mathbb{E}\left[\min\left(\frac{1}{k}\sum_{j=1}^{M}\mathbf{1}_{x_j^s \in B(x_1^r, \mathrm{NND}_k^r(x_1^r))}, 1\right)\right] \\
&= \frac{1}{k}\mathbb{E}\left[\min\left(\underbrace{\sum_{j=1}^{M}\mathbf{1}_{x_j^s \in B(x_1^r, \mathrm{NND}_k^r(x_1^r))}}_{\#\{\text{synthetic samples in } x_1^r\text{'s ball}\}}, k\right)\right] \\
&= \frac{1}{k}\mathbb{E}\left[\underbrace{\sum_{k'=1}^{k}\mathbf{1}_{\mathrm{NN}_{k'}^s(x_1^r) \in B(x_1^r, \mathrm{NND}_k^r(x_1^r))}}_{\substack{\text{how many of the } k\text{-nearest synthetic samples} \\ \text{of } x_1^r \text{ are within its ball}}}\right] \\
&= \frac{1}{k}\sum_{k'=1}^{k}\mathbb{P}\left(\mathrm{NN}_{k'}^s(x_1^r) \in B(x_1^r, \mathrm{NND}_k^r(x_1^r))\right)
\end{aligned}$$

We apply the linearity of expectation in lines 1, 2, and 4, and use the i.i.d. hypothesis for the x_i^r in line 1. For line 3, we use the fact that the number of synthetic samples within the ball of x_1^r, when limited to k, is equal to the number of synthetic samples among the k-nearest synthetic neighbors of x_1^r that fall within that ball. Here, NN_k^r denotes the k-th nearest real data sample, while $\mathrm{NN}_{k'}^s$ denotes the k'-th nearest synthetic data sample.

Let $S^r = \{\|x_i^r - x_1^r\|\}_{i=2}^{N}$ be the set of real distances to x_1^r, and let S_k^r be the k-th order statistic of S^r (i.e., the k-th smallest element): $S_k^r = \|\mathrm{NN}_k^r(x_1^r) - x_1^r\|$. Similarly, let $S^s = \{\|x_j^s - x_1^r\|\}_{j=1}^{M}$ be the set of synthetic distances to x_1^r, and let S_k^s be the k-th order statistic of S^s: $S_k^s = \|\mathrm{NN}_k^s(x_1^r) - x_1^r\|$. Let C_k^1 be the number of synthetic samples contained in the k-ball of x_1^r.

$$\begin{aligned}
\mathbb{P}\left(\mathrm{NN}_{k'}^s(x_1^r) \in B(x_1^r, \mathrm{NND}_k^r(x_1^r))\right) &= \mathbb{P}\left(\|\mathrm{NN}_{k'}^s(x_1^r) - x_1^r\| \leq \|\mathrm{NN}_k^r(x_1^r) - x_1^r\|\right) \\
&= \mathbb{P}\left(S_{k'}^s \leq S_k^r\right) \\
&= \mathbb{P}\left(k' \leq C_k^1\right)
\end{aligned}$$

S_k^r divides the population into two parts: k elements $\leq S_k^r$ and $N-1-k$ elements $> S_k^r$. Since the real and synthetic distributions are the same, for a fixed S_k^r, C_k^1 follows a binomial distribution with parameters: number of trials M and probability of success equal to $F(S_k^r)$, where F is the CDF of the random variable $\|X - x_1^r\|$, with $X \sim p_r$. Thus, $C_k^1 | S_k^r \sim \text{Binomial}(M, F(S_k^r))$.

Since S_k^r is random, so is $F(S_k^r)$. For any continuous distribution Y, $F(Y)$ is uniform (Embrechts & Hofert, 2013). Because the CDF is monotonically increasing, $F(S_k^r)$, the CDF of the k-th order statistic of S^r, is the k-th smallest element of the set $F(S^r)$: $F(S_k^r) = F(S^r)_k$. The k-th order statistic of a uniform distribution follows a Beta distribution (Gentle, 2009), so we have: $F(S_k^r) \sim \text{Beta}(k, (N-1)-k+1) \sim \text{Beta}(k, N-k)$.

When the success probability of a binomial distribution is itself a random variable following a Beta distribution, the resulting distribution is a Beta-Binomial distribution: $C_k^1 \sim \text{Beta-Binomial}(M, k, N-k)$.

Let β be the beta function:

$$\mathbb{P}(k' \leq C_k^1) = \sum_{j=k'}^{M}\binom{M}{j}\frac{\beta(k+j, M-j+N-k)}{\beta(k, N-k)}$$

$$\frac{1}{k}\sum_{k'=1}^{k}\mathbb{P}\left(\mathrm{NN}^s_{k'}(x^r_1) \in B(x^r_1, \mathrm{NND}^r_k(x^r_1))\right) = \frac{1}{k}\sum_{k'=1}^{k}\sum_{j=k'}^{M}\binom{M}{j}\frac{\beta(k+j, M-j+N-k)}{\beta(k, N-k)}$$
$$= \frac{1}{k}\sum_{j=1}^{M}\sum_{k'=1}^{\min(j,k)}\binom{M}{j}\frac{\beta(k+j, M-j+N-k)}{\beta(k, N-k)}$$
$$= \sum_{j=1}^{M}\min\left(\frac{j}{k}, 1\right)\binom{M}{j}\frac{\beta(k+j, M-j+N-k)}{\beta(k, N-k)}$$

□

B Implementation details

B.1 Clipped Coverage

To compute f_{expected} efficiently for all m, we begin by precomputing log-gamma values for all integers l between 1 and $M + N + 1$. Then, all required beta values and binomial coefficients can be computed as differences of three precomputed log-gamma values: $\log$-Beta$(a, b) = \log$-Gamma$(a) + \log$-Gamma$(b) - \log$-Gamma$(a + b)$ and $\log$-$\binom{n}{k} = \log$-Gamma$(n + 1) - \log$-Gamma$(k + 1) - \log$-Gamma$(n - k + 1)$.

For the computation of Clipped Coverage, we take an approach similar to that used in the proof of Lemma 1: we count how many of the k-closest synthetic samples to a real sample are contained within its ball. This can be computed using only nearest neighbor searches, which is more efficient than searching for all synthetic samples within the ball of each real sample.

B.2 Comparison with existing metric implementations

We compare our implementation with the implementations of:

- *Precision*, *Recall*, *Density*, and *Coverage* by Naeem et al. (2020) (`https://github.com/clovaai/generative-evaluation-prdc/blob/master/prdc/prdc.py`)
- *symPrecision* and *symRecall* by Khayatkhoei & AbdAlmageed (2023) (`https://github.com/mahyarkoy/emergent_asymmetry_pr/blob/main/manifmetric/manifmetric.py`)
- *P-precision* and *P-recall* by Park & Kim (2023) using GPU (`https://github.com/kdst-team/Probablistic_precision_recall/blob/master/metric/pp_pr.py`)
- Our own implementation of *Precision Recall Cover*, following the pseudocode in Appendix A.3 of the original paper (Cheema & Urner, 2023)

Our implementation simultaneously computes *Precision*, *Recall*, *Density*, and *Coverage*, with optional computation of *symPrecision*, *symRecall*, *P-precision*, and *P-recall*. Since some intermediary computations are shared between these metrics, we compute them once and reuse them. We compute *Precision Recall Cover* separately because the k value used differs from the other metrics ($k' = 3$ instead of $k = 5$, see Section 5).

In the original implementations, the number of parallel threads is sometimes hardcoded to 8, so for a fair comparison, we use only 8 of the 24 threads available on our hardware, which is an H100 GPU with 80GB of RAM (as stated in Section 5).

We run the implementations on sets of 10000 standard Gaussians in dimension 32 and on the DINOv2 embedding of FFHQ with the synthetic set generated by the Latent Diffusion Model (LDM), hereafter "DINOv2-FFHQ-LDM", for a total of 50000 samples in both the real and synthetic sets. The results are shown in Table 1.

Table 1: **Implementation comparison**

	10000 standard Gaussians, $d = 32$				DINOv2-FFHQ-LDM			
	Values		Time (s)		Values		Time (min)	
Metric name	Initial	Ours	Initial	Ours	Initial	Ours	Initial	Ours
Precision	0.7706	0.7706	3.93	8.43	0.7352	0.7352	2.05	25.2
Recall	0.7764	0.7764			0.3969	0.3969		
Density	0.9591	0.9591			0.6475	0.6475		
Coverage	0.9645	0.9645			0.5817	0.5817		
symPrecision	0.7706	0.7706	17.3		0.3267	0.3267	157	
symRecall	0.7764	0.7764			0.3969	0.3969		
P-precision	0.9251	0.9251	1.66		DNF	0.7229	DNF	
P-recall	0.9249	0.9249			DNF	0.6896		
Precision Cover	0.9553	0.9553	55.7	2.23	0.1785	0.1785	88.2	2.90
Recall Cover	0.9357	0.9357	61.0	2.25	0.4637	0.4637	67.9	2.99

When both the original and our implementations finish, we obtain the exact same values. The original implementation of *P-precision* and *P-recall* does not finish (DNF) on the FFHQ test due to memory issues.

The main difference between our implementation and the existing ones is the use of Scikit-learn's (Pedregosa et al., 2011) `NearestNeighbors` method for the nearest neighbor search. We also use it for ball tree radius queries, which find all samples within a given radius of a specific point.

For simplicity, we assume here that the number of real and synthetic samples is the same: $N = M$. Ball trees are built in $O(dN \log N)$ time and $O(Nd)$ space (Omohundro, 1989; Huang & Tung, 2023) for N samples in dimension d, while queries take $O(d \log N)$ operations in low dimensions and up to $O(dN)$ time in high dimensions (Liu et al., 2006) (note that this query is performed N times).

In contrast, initial implementations usually compute the distances between all pairs of samples and search through these distances instead. The construction complexity is then $O(dN^2)$ time and $O(N^2)$ space. Finding all points within a given radius of a specific point can then be done in $O(N)$ time because the distances are already computed.

Our method therefore has at most the same time complexity as the initial implementation, but with memory usage of $O(Nd)$ instead of $O(N^2)$.

For DINOv2-FFHQ-LDM, where $N = 50000$ and $d = 1024$, the original *P-precision* and *P-recall* implementation fails due to out-of-memory errors, as it attempts to allocate an additional 24GB of RAM on top of the 73GB already in use ($73 = 24 \times 3 + 1$). This implementation stores four pairwise distance matrices, whereas `prdc.py` (for *Precision*, *Recall*, *Density*, and *Coverage*) stores only one.

B.3 Computational requirements

The approximate computation times for the experiments were as follows:

- Extracting DINOv2 embeddings took 3.7 minutes per dataset. With 46 datasets in total ($14 + 12 + 10 + 10$), this amounted to 2.8 hours.
- For synthetic data tests (25000 samples, dimension $d = 32$), each evaluation of all metrics took 8 minutes. The total computation time for these tests, encompassing various scenarios and repetitions ($21 \times 5 + (11 + 11/2 + 4) \times 10$), was 41 hours.
- For real tests using DINOv2 embeddings of CIFAR-10 (25000 samples, dimension $d = 1024$), each evaluation of all metrics took 13.7 minutes. The total computation time for these tests ($(11 + 11/2 + 4) \times 10$) was 47 hours.

- The evaluation of generative models on real datasets took 40 minutes per generated set. With 42 generated sets evaluated $(13 + 11 + 9 + 9)$, this totaled 28 hours.

Overall, reproducing all the experimental results presented in this paper would require approximately 120 hours of computation time. The complete research project, including preliminary experiments and explorations not detailed in the final paper, required an estimated 200-300 hours of computation time.

C Datasets

C.1 Real data for metric evaluation tests

For tests conducted on real data, the samples are DINOv2 embeddings derived from the CIFAR-10 dataset (Krizhevsky et al., 2009). When a test requires out-of-distribution (or "bad") samples, these are DINOv2 embeddings of Gaussian noise images.

C.2 Generated datasets

This section details the generated datasets evaluated in Figures 6, 12 and 13. All data were publicly shared by Stein et al. (2023) through the link provided in their GitHub repository: `https://github.com/layer6ai-labs/dgm-eval`. For more information on the generation process, see Appendix A of Stein et al. (2023).

We used 50000 samples for each evaluation. For conditional models, an equal number of samples per class was taken, except when only 50000 unbalanced images were available.

C.2.1 CIFAR-10

For CIFAR-10 (Krizhevsky et al., 2009), data were generated using the following models:

- LSGM-ODE (Vahdat et al., 2021)
- PFGM++ (PFGMPP) (Xu et al., 2023)
- iDDPM-DDIM (Nichol & Dhariwal, 2021)
- StudioGAN models (Kang et al., 2023a)
  - ACGAN-Mod (Odena et al., 2017)
  - BigGAN (Brock et al., 2019)
  - LOGAN (Wu et al., 2019)
  - MHGAN (Turner et al., 2019)
  - ReACGAN (Kang et al., 2021)
  - WGAN-GP (Gulrajani et al., 2017)
- StyleGAN-XL (Sauer et al., 2022)
- StyleGAN2-ada (Karras et al., 2020)
- RESFLOW (Chen et al., 2019)
- NVAE (Vahdat & Kautz, 2020)

C.2.2 ImageNet

For ImageNet (Deng et al., 2009), images were rescaled to 256×256 using center cropping followed by bicubic interpolation downsampling before being shared by Stein et al. (2023). The synthetic data were generated using the following models:

- Models for which datasets of 50000 unbalanced samples were initially shared by Dhariwal & Nichol (2021):
  - ADM (Dhariwal & Nichol, 2021)
  - ADMG (Dhariwal & Nichol, 2021)

  - ADMG-ADMU (Dhariwal & Nichol, 2021)
  - BigGAN (Brock et al., 2019)
- DiT-XL-2 (Peebles & Xie, 2023)
- DiT-XL-2-guided (Peebles & Xie, 2023)
- LDM (Rombach et al., 2022)
- GigaGAN (Kang et al., 2023b)
- StyleGAN-XL (Sauer et al., 2022)
- Mask-GIT (Chang et al., 2022)
- RQ-Transformer (Lee et al., 2022)

C.2.3 LSUN Bedroom

For LSUN Bedroom (Yu et al., 2015), data were generated using the following models:

- Consistency (Song et al., 2023). We used the two sets provided by Stein et al. (2023), referred to as Consistency-set1 and Consistency-set2.
- Four models for which datasets of 50000 unbalanced samples were originally shared by Dhariwal & Nichol (2021):
  - ADM-dropout (Dhariwal & Nichol, 2021)
  - DDPM (Ho et al., 2020)
  - iDDPM (Nichol & Dhariwal, 2021)
  - StyleGAN (Karras et al., 2019)
- Diff-ProjGAN: Diffusion-Projected GAN (Wang et al., 2023)
- Projected GAN (Sauer et al., 2021)
- Unleash-Trans: Unleashing Transformers (Bond-Taylor et al., 2022)

C.2.4 FFHQ

For FFHQ (Kazemi & Sullivan, 2014), images were downsampled to 256×256 using Lanczos interpolation before being shared by Stein et al. (2023). The data were generated using the following models:

- LDM (Rombach et al., 2022)
- InsGen (Yang et al., 2021)
- Projected-GAN (Sauer et al., 2021)
- StyleGAN-XL (Sauer et al., 2022)
- StyleGAN2-ada (Karras et al., 2020)
- StyleNAT (Walton et al., 2022)
- StyleSwin (Zhang et al., 2022)
- Unleash-Trans: Unleashing Transformers (Bond-Taylor et al., 2022)
- Efficient-vdVAE (Hazami et al., 2022)

D EXAMPLE OF REAL OUT-OF-DISTRIBUTION SAMPLES INFLATING *Density*

The RESFLOW-generated CIFAR-10 dataset achieves a *Density* of 2.47, a value inflated by real out-of-distribution samples. To investigate this, we categorized real samples by counting the number of synthetic samples within their 5-ball (Table 2).

Table 2: **Synthetic points per real k-ball (RESFLOW CIFAR-10).**

Synthetic points in a real ball	Real balls (no clipping)	Real balls (with clipping)
0	48373	49981
1–5	680	15
6–100	513	3
101–1000	282	1
1001–10000	148	0
10001+	4	0

Without radii clipping, 48373 real balls contain no synthetic points, whereas just 4 contain over 10000. The 4 corresponding real images appear out-of-distribution (see Figure 7).

(a) Very gray ship image. (b) Camouflaged cat. (c) 2-legged horse. (d) Toy ship on a stand.

Figure 7: **Real CIFAR-10 samples containing more than** 10000 **synthetic points in their** 5**-ball**. These images are atypical for their classes. (a) A ship viewed from above, maybe at night, resulting in a mostly gray image. (b) A cat on top of a similarly colored object. (c) An unusually shaped horse that appears to have only two legs. (d) A toy ship on a stand instead of in water.

A real point having many synthetic points in its ball is not inherently problematic, as generative models might generate many similar images. However, in this case, these 4 images are outliers that artificially increase the measured fidelity by being very far from other points. Here, clipping the real balls is enough to make the measured fidelity drop to 0.00.

E FROM *Density* TO *Clipped Density*: OVER-OCCURRING SAMPLE PROPORTION AND RADII CLIPPING

This section measures the effects of the successive modifications that transform *Density* into *Clipped Density*. Below, we detail their impact on the evaluation of real generated datasets, along with the proportion of over-occurring samples (i.e., samples with a fidelity score greater than 1) at each step.

The columns, in order, present: the original *Density* score, the initial proportion of over-occurring samples (OOP), the *Density* score after radii clipping, the OOP after radii clipping, the scores after individual sample contributions are also clipped (resulting in $\text{ClippedDensity}_{\text{unnorm}}$), and finally, the fully normalized *ClippedDensity*.

Table 3: **From *Density* to *Clipped Density* on CIFAR-10.**

Model	Density	Initial OOP (%)	Density (clipped radii)	OOP (clipped radii) (%)	$\text{ClippedDensity}_{\text{unnorm}}$	ClippedDensity
LSGM-ODE	0.66	18.4	0.22	6.0	0.14	0.38
PFGMPP	0.65	18.3	0.22	6.3	0.15	0.39
iDDPM-DDIM	0.64	17.4	0.19	5.6	0.13	0.34
ACGAN-Mod	2.28	43.0	0.00	0.0	0.00	0.01
BigGAN	0.55	14.4	0.10	2.6	0.07	0.19
LOGAN	1.01	22.4	0.00	0.0	0.00	0.01
MHGAN	0.57	14.9	0.06	1.6	0.05	0.13
ReACGAN	0.57	14.2	0.07	1.6	0.05	0.14
StyleGAN-XL	0.58	15.3	0.15	4.0	0.10	0.27
StyleGAN2-ada	0.60	16.4	0.13	3.4	0.09	0.24
WGAN-GP	1.74	37.2	0.00	0.0	0.00	0.01
RESFLOW	2.47	47.4	0.00	0.0	0.00	0.00
NVAE	1.59	31.9	0.00	0.0	0.00	0.00

Table 4: **From *Density* to *Clipped Density* on ImageNet.**

Model	Density	Initial OOP (%)	Density (clipped radii)	OOP (clipped radii) (%)	$\text{ClippedDensity}_{\text{unnorm}}$	ClippedDensity
ADM	0.38	8.3	0.08	2.2	0.07	0.17
ADMG	0.49	12.8	0.17	4.7	0.13	0.34
ADMG-ADMU	0.55	15.5	0.21	5.8	0.16	0.41
DiT-XL-2	0.83	28.2	0.43	14.6	0.29	0.74
DiT-XL-2-guided	1.65	63.8	1.12	42.3	0.63	1.00
LDM	0.70	21.5	0.32	10.0	0.22	0.57
BigGAN	0.46	10.5	0.05	0.9	0.05	0.12
GigaGAN	0.41	9.2	0.07	1.5	0.06	0.15
StyleGAN-XL	0.38	8.3	0.06	1.2	0.05	0.13
Mask-GIT	0.43	10.3	0.10	2.2	0.09	0.22
RQ-Transformer	0.34	6.8	0.04	0.8	0.03	0.09

Table 5: **From *Density* to *Clipped Density* on LSUN Bedroom.**

Model	Density	Initial OOP (%)	Density (clipped radii)	OOP (clipped radii) (%)	ClippedDensity$_{\text{unnorm}}$	ClippedDensity
Consistency-set1	0.62	18.7	0.14	3.4	0.11	0.32
Consistency-set2	0.64	18.9	0.13	2.9	0.11	0.30
ADM-dropout	0.83	25.9	0.41	12.6	0.26	0.73
DDPM	0.55	14.5	0.16	4.6	0.11	0.32
iDDPM	0.64	18.2	0.23	6.8	0.16	0.44
Diff-ProjGAN	0.56	15.0	0.05	1.1	0.05	0.13
Projected-GAN	0.63	16.9	0.05	0.9	0.04	0.12
StyleGAN	0.74	21.8	0.26	7.4	0.17	0.48
Unleash-Trans	0.51	12.5	0.06	1.4	0.05	0.14

Table 6: **From *Density* to *Clipped Density* on FFHQ.**

Model	Density	Initial OOP (%)	Density (clipped radii)	OOP (clipped radii) (%)	ClippedDensity$_{\text{unnorm}}$	ClippedDensity
LDM	0.65	18.4	0.24	6.6	0.16	0.41
InsGen	0.32	6.9	0.06	1.3	0.05	0.12
Projected-GAN	0.21	3.5	0.02	0.2	0.01	0.03
StyleGAN-XL	0.51	13.0	0.14	3.6	0.10	0.26
StyleGAN2-ada	0.24	4.2	0.04	0.7	0.03	0.08
StyleNAT	0.61	16.5	0.20	5.3	0.14	0.35
StyleSwin	0.53	13.8	0.13	3.1	0.10	0.25
Unleash-Trans	0.46	11.0	0.10	2.5	0.08	0.19
Efficient-vdVAE	0.80	23.2	0.28	7.9	0.17	0.42

F Evaluation of Generated Chest X-Rays

We evaluated a Progressively Growing GAN (Karras et al., 2018) from the Medigan library (Osuala et al., 2023), trained by Segal et al. (2021) on the ChestX-ray8 dataset (Wang et al., 2017) (≈ 110000 chest X-ray images). The model yielded a *Clipped Density* of 0.06 and a *Clipped Coverage* of 0.03.

The absolute interpretability of our metrics allows a direct assessment of these results without requiring comparison to other models. A *Clipped Density* of 0.06 implies that the model's output has a fidelity equivalent to a dataset composed of only 6% good samples and 94% bad samples; similarly, a *Clipped Coverage* of 0.03 is equivalent to a dataset with only 3% good samples.

This is a critical advantage over relative metrics, which can only rank models against each other without revealing whether even the best-performing one is adequate for a given task. In high-stakes domains like medical imaging, the ability to make an absolute judgment is essential. A low score provides a clear, unambiguous signal that the model is not yet fit for purpose, preventing the premature adoption of a technology that fails to meet the necessary standards for safety and reliability.

G Fidelity under Imputed Distortions

To further assess the behavior of *Clipped Density*, we evaluated the fidelity of PFGMPP-generated CIFAR-10 samples under various image distortions, replicating the setup from Figure 5 of Jiralerspong et al. (2023). Our results for *Clipped Density*, shown in Figure 8, align with those reported for the Feature Likelihood Divergence (FLD) metric in the original study, which were themselves better than those of FID.

We applied the transformations detailed in Appendix E.1 of Jiralerspong et al. (2023). For the Color Distort transformation, the default parameters produce an identity transform, so we used a non-default `hue = 0.3`. For the Center Crop transformation, two different values (28 and 30) are used throughout the paper. We proceeded with the value 28.

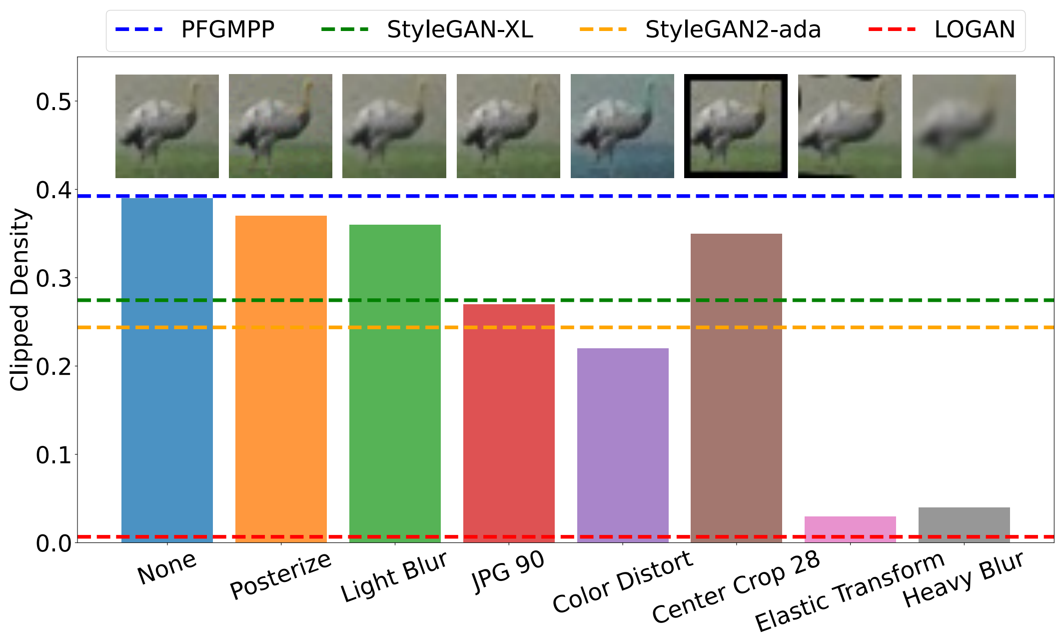

Figure 8: **Fidelity of PFGMPP samples under different image distortions, measured with *Clipped Density*.** Horizontal lines represent the *Clipped Density* scores of other models for comparison.

H Comparison to a Recent Benchmark

A recent position paper by Räisä et al. (2025) argues that ”all current generative fidelity and diversity metrics are flawed” and that ”no metric is suitable for absolute evaluations.” Our work tackles these issues directly. In this section, we evaluate *Clipped Density* and *Clipped Coverage* on the benchmark from Räisä et al. (2025), using the authors' original code. All tests in this benchmark are performed on synthetic data, with a default sample size of 1000.

The results are summarized in Tables 7 and 8, which reproduce the tables from Räisä et al. (2025) with *Clipped Density* (Cl-Dens) and *Clipped Coverage* (Cl-Cov) added for comparison. Here, T denotes a passed test, while F indicates failure. The original benchmark distinguishes between high (H, support-based) and low (L, density-based) diversity metrics. Since we aim to measure coverage, which assesses densities, we interpret L as a success (T) and H as a failure (F).

We observed seven discrepancies with the original results, marked with a royal blue underline (T or F). These differences arise from the benchmark's seed generation: the seed is based on a hash of the metric name, test name, and repetition index, but Python's built-in `hash` function changes across different sessions unless `PYTHONHASHSEED` is set. As a result, seeds (and thus results) differ between runs.

Table 7: **Fidelity metrics comparison on a recent benchmark from Räisä et al. (2025)**

Desiderata	Sanity Check	I-Prec	Density	IAP	C-Prec	symPrec	P-Prec	Cl-Dens
Purpose	Discrete Num. vs. Continuous Num.	F	F	F	F	F	F	F
	Gaussian Mean Difference	T	T	T	T	T	T	T
	Gaussian Mean Difference + Outlier	F	T	T	T	F	T	T
	Gaussian Mean Difference + Pareto	T	T	T	T	T	T	T
	Gaussian Std. Deviation Difference	T	T	F	F	F	T	T
	Hypercube, Varying Sample Size	F	F	F	F	F	F	F
	Hypercube, Varying Syn. Size	F	F	F	F	F	F	F
	Hypersphere Surface	F	F	T	F	T	F	F
	Mode Collapse	T	T	T	T	T	T	T
	Mode Dropping + Invention	T	T	F	F	F	T	T
	One Disjoint Dim. + Many Identical Dim.	F	F	F	F	F	F	F
	Sequential Mode Dropping	T	T	F	F	F	T	T
	Simultaneous Mode Dropping	T	F	F	F	F	T	T
	Sphere vs. Torus	T	T	T	F	T	T	T
Hyperparam.	Hypercube, Varying Syn. Size	T	T	T	F	F	T	T
Data	Hypercube, Varying Sample Size	F	F	F	F	F	F	F
Bounds	Discrete Num. vs. Continuous Num.	F	F	F	F	F	F	F
	Gaussian Mean Difference	F	T	F	T	F	F	T
	Gaussian Mean Difference + Outlier	F	F	F	T	F	F	F
	Gaussian Mean Difference + Pareto	F	T	T	T	T	F	T
	Gaussian Std. Deviation Difference	F	F	F	F	F	F	F
	Hypersphere Surface	F	F	F	F	T	F	F
	Mode Collapse	F	T	F	T	F	F	T
	Mode Dropping + Invention	T	T	F	F	F	F	T
	One Disjoint Dim. + Many Identical Dim.	F	F	T	F	F	F	F
	Scaling One Dimension	T	T	T	T	T	T	T
	Sequential Mode Dropping	F	T	F	F	F	F	T
	Simultaneous Mode Dropping	F	F	F	F	F	F	T
	Sphere vs. Torus	T	T	F	F	T	T	T
Invariance	Scaling One Dimension	F	T	T	T	T	T	T

Table 8: **Coverage metrics comparison on a recent benchmark from Räisä et al. (2025)**

Desiderata	Sanity Check	I-Rec	Coverage	IBR	C-Rec	symRec	P-Rec	Cl-Cov
Purpose	Discrete Num. vs. Continuous Num.	F	F	F	F	F	F	F
	Gaussian Mean Difference	T	T	T	T	T	T	T
	Gaussian Mean Difference + Outlier	F	T	T	T	T	T	T
	Gaussian Mean Difference + Pareto	T	T	T	T	T	T	T
	Gaussian Std. Deviation Difference	H	F	L	F	F	H	F
	Hypercube, Varying Sample Size	F	F	F	F	F	F	F
	Hypercube, Varying Syn. Size	F	F	F	F	F	F	F
	Hypersphere Surface	F	F	F	F	T	F	F
	Mode Collapse	F	F	F	F	F	F	L
	Mode Dropping + Invention	T	F	F	F	F	T	*F*
	One Disjoint Dim. + Many Identical Dim.	F	F	F	F	F	F	F
	Sequential Mode Dropping	T	T	F	F	T	T	T
	Simultaneous Mode Dropping	F	T	F	T	F	T	T
	Sphere vs. Torus	F	F	F	F	F	F	T
Hyperparam.	Hypercube, Varying Syn. Size	F	F	F	F	F	F	F
Data	Hypercube, Varying Sample Size	F	F	F	F	F	F	F
Bounds	Discrete Num. vs. Continuous Num.	F	F	F	F	F	F	F
	Gaussian Mean Difference	F	T	F	T	F	F	F
	Gaussian Mean Difference + Outlier	F	T	F	T	F	F	T
	Gaussian Mean Difference + Pareto	F	T	F	T	T	F	T
	Gaussian Std. Deviation Difference	F	F	F	F	F	F	F
	Hypersphere Surface	F	F	F	F	T	F	F
	Mode Collapse	F	T	F	T	F	F	F
	Mode Dropping + Invention	T	F	F	F	F	F	*F*
	One Disjoint Dim. + Many Identical Dim.	F	F	T	F	F	F	F
	Scaling One Dimension	F	T	T	T	T	T	T
	Sequential Mode Dropping	F	T	F	T	F	F	T
	Simultaneous Mode Dropping	F	T	F	T	F	F	T
	Sphere vs. Torus	T	F	F	T	F	T	T
Invariance	Scaling One Dimension	F	T	T	T	T	T	T

Purple underlined entries (F) indicate cases where the benchmark's criterion for success is, in our view, overly strict (see Appendix H.1). Italic blue entries (*F*) indicate cases where the original implementation counts a failure, but we argue that for low diversity metrics, these should be considered successes (see Appendix H.2).

H.1 HARSH CRITERIA

Purple underlined entries (F) correspond to cases where, in our view, the benchmark's threshold for passing may be too narrow.

In the "Gaussian Mean Difference" test (Figure 9), which is analogous to our synthetic Gaussian translation test but without bad samples, the bounds desideratum is not satisfied by *Clipped Coverage* in dimension 64 with no translation (0). In this case, the initial and synthetic distributions are the same. *Clipped Coverage* has a value of 0.947, while the criterion requires a value between 0.95 and 1.05.

Similarly, in the "Mode Collapse" test (Figure 10), where real data is a mixture of two Gaussians spaced by μ and the synthetic data is a single Gaussian, the value in dimension 64 with no translation (0, same initial and synthetic distributions) is 0.941, just below the same required threshold.

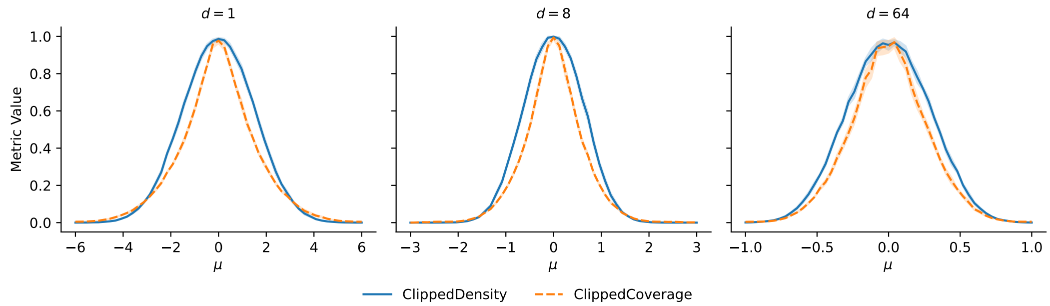

Figure 9: **Gaussian Mean Difference**: output from the original code for our metrics.

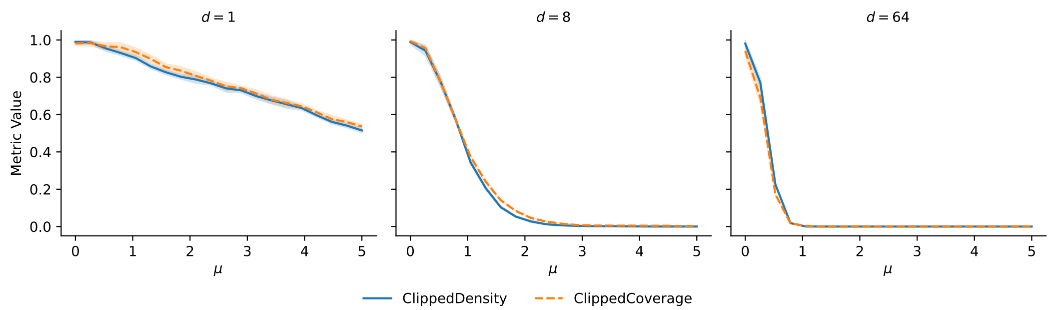

Figure 10: **Mode Collapse**: output from the original code for our metrics.

H.2 Incorrect criterion

Italic blue entries (*F*) indicate cases where we disagree with the benchmark's failure criterion.

In the "Mode Dropping + Invention" test (Figure 11), the real data is a mixture of 5 Gaussians, and the synthetic data progressively includes the 5 real modes and then 5 invented modes. Both real and synthetic sets always have 1000 samples.

Clipped Coverage is marked as failing because it decreases when invented modes are added. However, this decrease is expected for low-diversity metrics (density-based): when invented modes are included, real modes become under-covered as the total amount of synthetic data remains the same, so coverage metrics should decrease. Thus, this behavior should be considered T or L, both successes for coverage metrics.

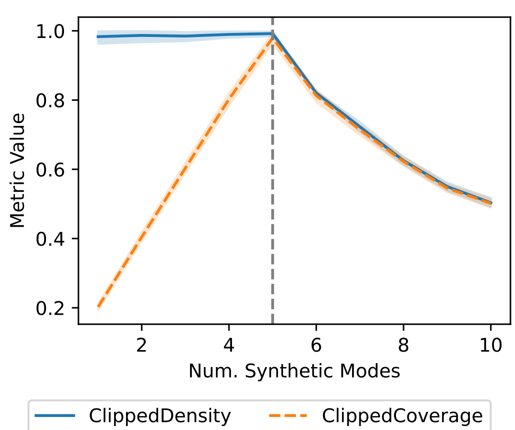

Figure 11: **Mode Dropping + Invention**: output from the original code for our metrics.

I Fidelity vs Coverage with other metrics

We reproduce Figure 6 with other metrics in Figures 12 and 13.

Several metric pairs show limited discrimination by the fidelity metric, with most variation captured by the coverage metric. This occurs for *Precision/Recall* (CIFAR-10, LSUN Bedroom), *TopP/TopR* (ImageNet, FFHQ), *P-precision/P-recall* (FFHQ), and *Precision Cover/Recall Cover* (FFHQ).

symPrecision and *symRecall* are highly correlated across all datasets. α-*Precision* and β-*Recall* show distinct results for consistency models on LSUN Bedroom, but their scores are generally confined to the lower-right quadrant.

Overall, these alternative metrics often exhibit limitations, such as poor discriminative power in fidelity scores, high correlation between fidelity and coverage, or restricted score ranges, hindering comprehensive assessment.

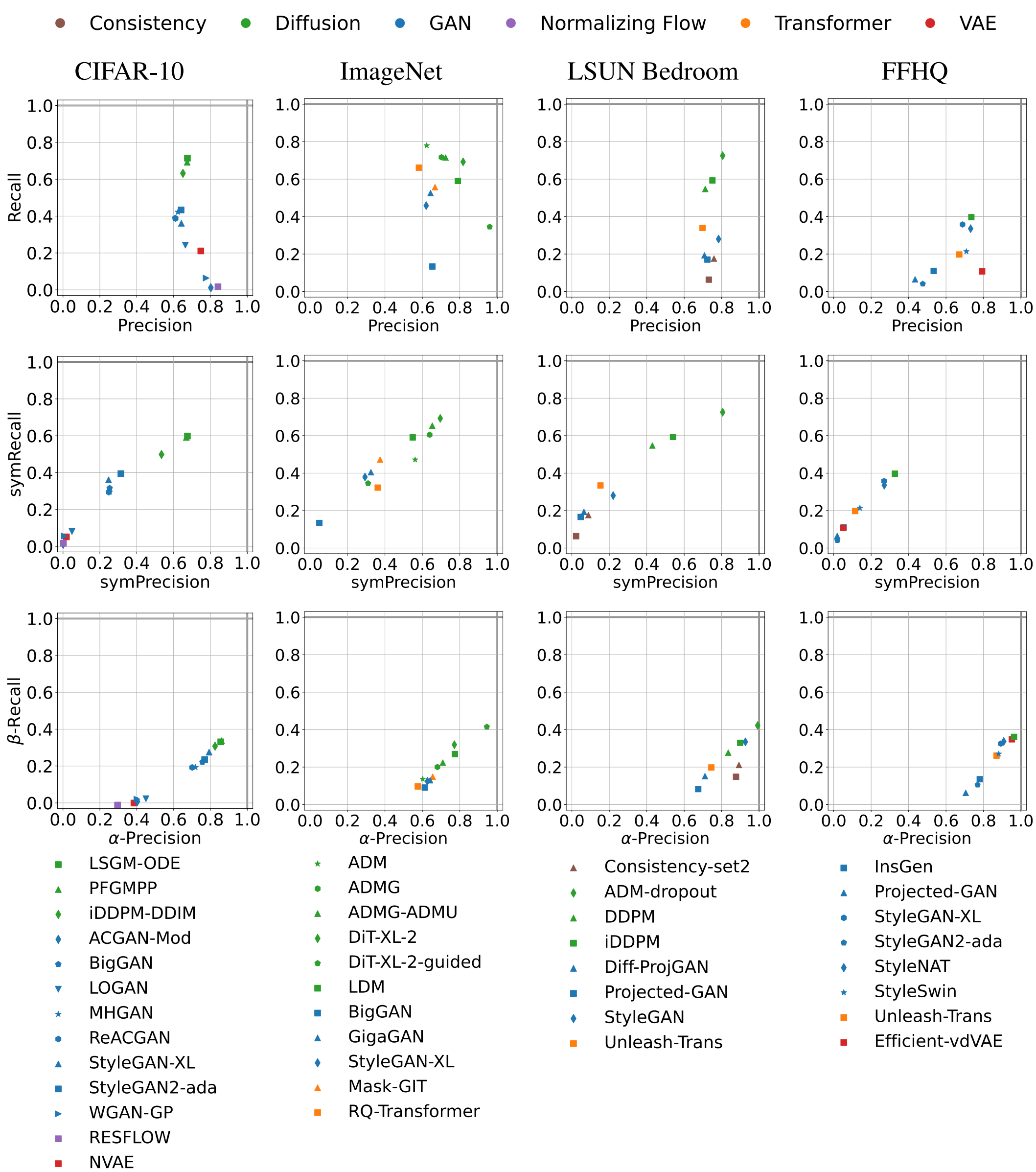

Figure 12: **Fidelity vs Coverage on various datasets, other metrics (1/2)**

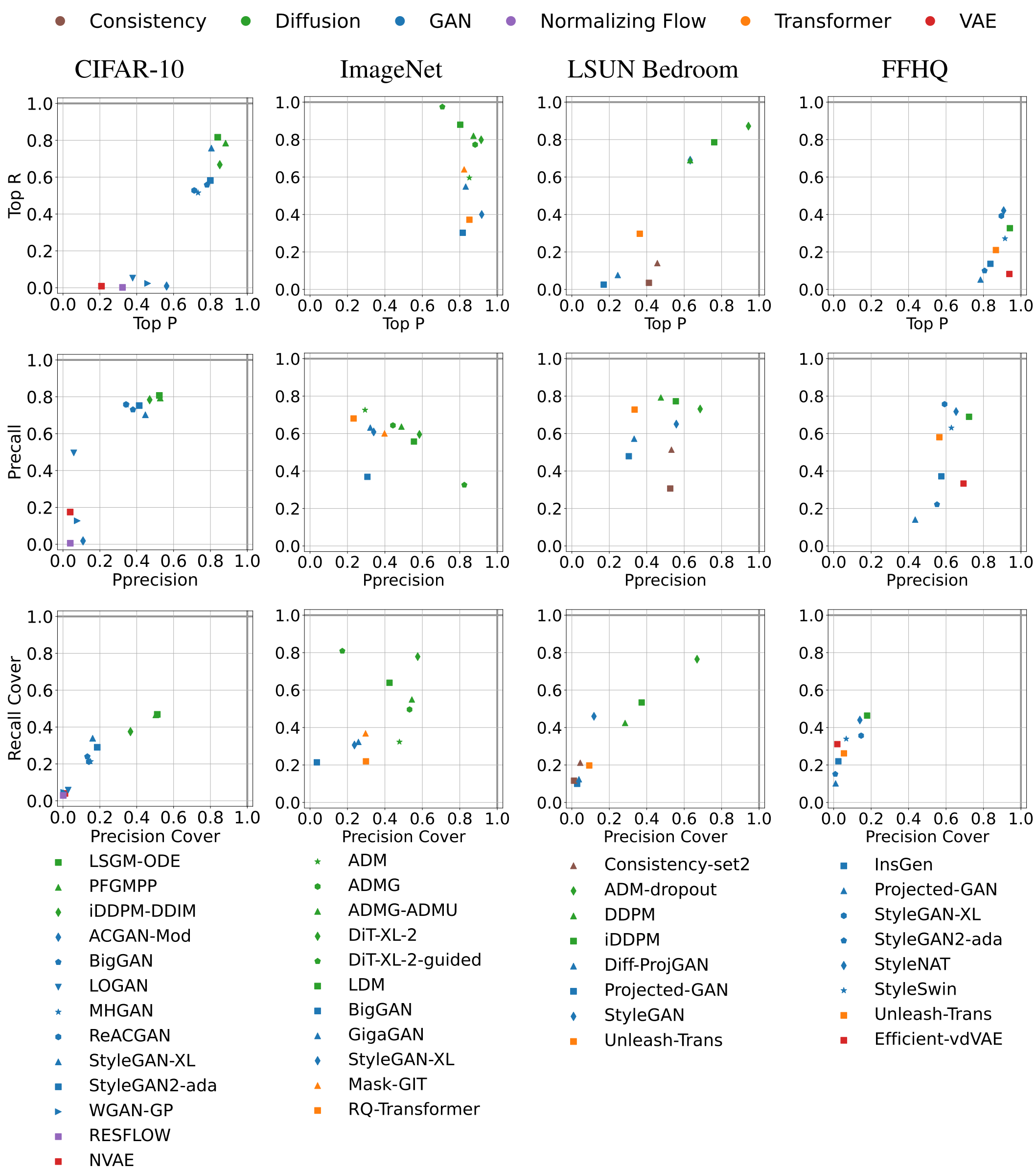

Figure 13: **Fidelity vs Coverage on various datasets, other metrics (2/2)**

J METRIC TESTS ON TOY DATASETS

This section details experiments on synthetic Gaussian data ($N = 25000, d = 32$, 10 repetitions), analogous to the CIFAR-10 tests in Section 5. Out-of-distribution samples are drawn from a Gaussian distribution with variance $\max(4, (10 + Z)^2)$, where $Z \sim \mathcal{N}(0, 1)$. The tests performed are:

- **Simultaneous mode dropping**: Progressively replacing data from all but one class with data from the remaining class (see Figure 14b, analogous to Figure 4b).
- **Matched real and synthetic out-of-distribution samples**: Progressively replacing data from both real and synthetic datasets with out-of-distribution samples (see Figures 14c and 15b, analogous to Figures 4c and 5a).
- **Introducing bad synthetic samples**: Progressively replacing synthetic data with out-of-distribution samples (see Figures 14a and 15a, analogous to Figures 1 and 4a).

J.1 FIDELITY METRICS

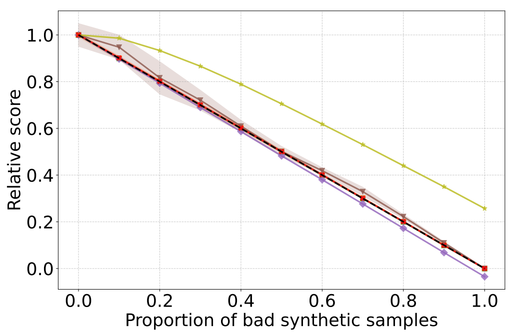

(a) Fidelity reduction with bad samples

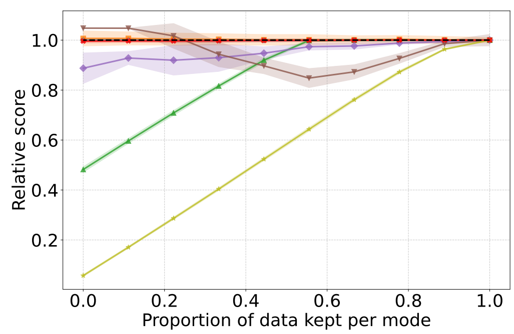

(b) Simultaneously dropping modes

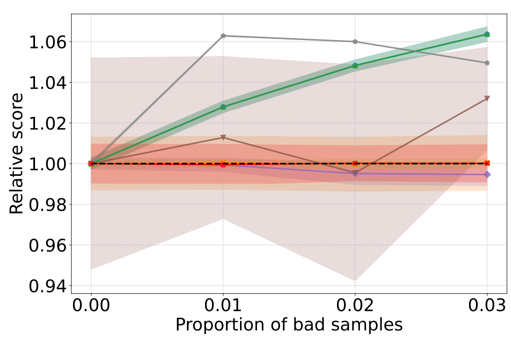

(c) Introducing bad real & syn. samples

Legend	Figure 14a	Figure 14b	Figure 14c	Figure 4d
Precision	✓	✓	✗	✗
Density	✓	✓	✓	✗
symPrecision	✓	✗	✗	✗
α-Precision	✓	✗	✗	✗
TopP	✓	✗	✗	✓
Pprecision	✓	✓	✗	✗
PrecisionCover	✗	✗	✓	✓
ClippedDensity (ours)	✓	✓	✓	✓
Ideal				

(d) Legend and summary

Figure 14: **Testing fidelity metrics on toy data**: this figure is the equivalent of Figure 4 on toy data.

J.2 Coverage metrics

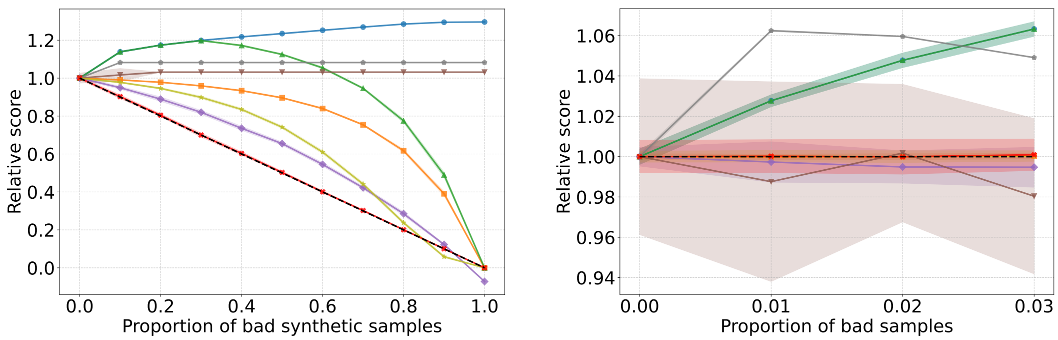

(a) Coverage reduction with bad samples (b) Introducing bad real & syn. samples

Legend	Figure 15a	Figure 15b	Figure 5b
Recall	✗	✓	✗
Coverage	✗	✓	✓
symRecall	✗	✗	✗
β-Recall	✗	✗	✗
TopR	✗	✗	✓
Precall	✗	✗	✗
RecallCover	✗	✓	✓
ClippedCoverage (ours)	✓	✓	✓
Ideal			

(c) Legend and summary

Figure 15: **Testing coverage metrics on toy data**: this figure is the equivalent of Figure 5 on toy data.

K Sensitivity to the hyperparameter k

The number of nearest neighbors, k, is a hyperparameter for *Clipped Density*, *Clipped Coverage*, and several other metrics. We evaluate their sensitivity to k on the DINOv2-FFHQ-LDM dataset (see the Figure below).

Scores increase with k, as this results in larger k-nearest neighbor balls and thus a higher likelihood of sample inclusion within these balls. *Clipped Density* and *Clipped Coverage* remain relatively stable, likely due to the normalization of the balls by their volume or mass.

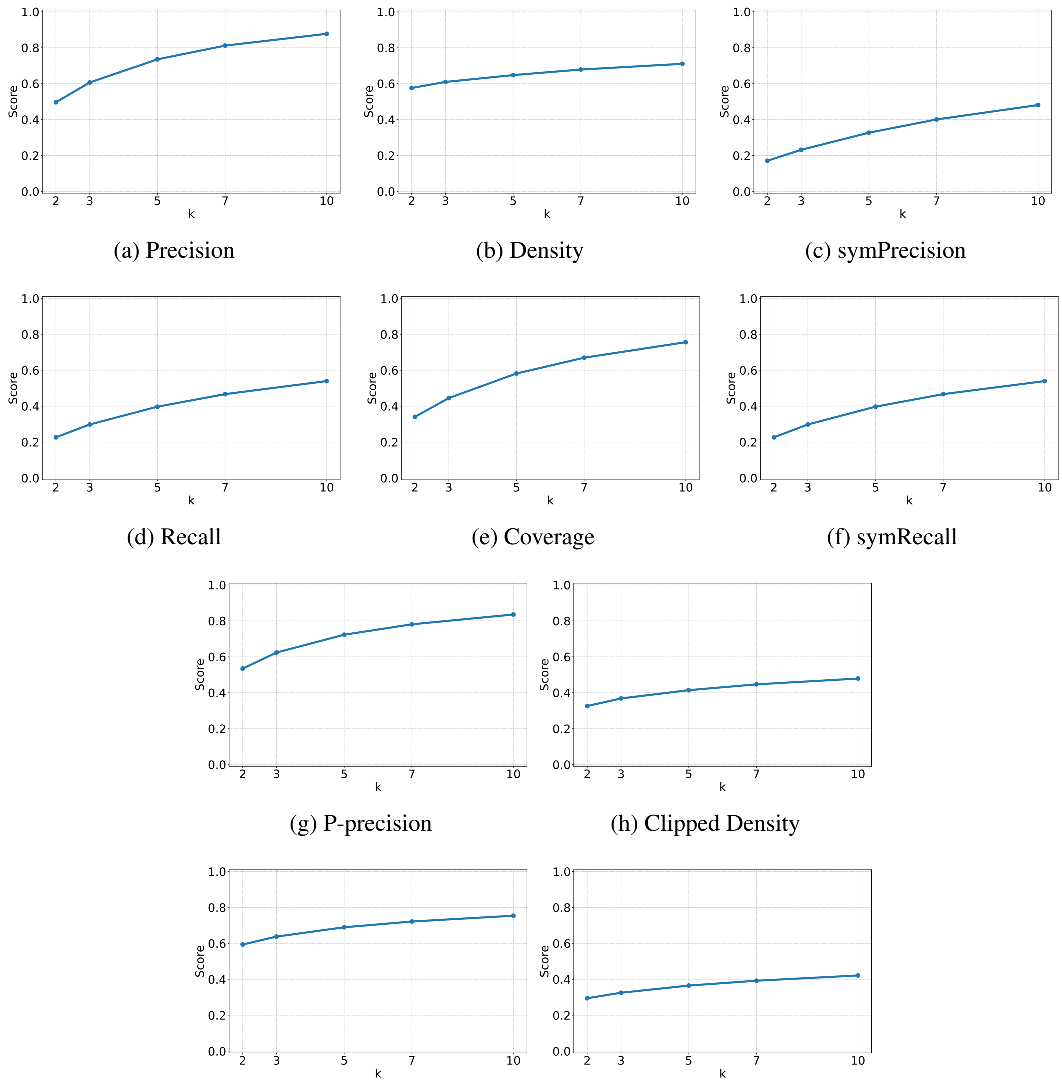

(a) Precision (b) Density (c) symPrecision

(d) Recall (e) Coverage (f) symRecall

(g) P-precision (h) Clipped Density

(i) P-recall (j) Clipped Coverage

Figure 16: **Sensitivity to** k on DINOv2-FFHQ-LDM.

L UNNORMALIZED RESULTS

Figures 1, 4 and 5 present relative scores. This section shows the corresponding unnormalized scores, which include the maximum values and can be easier to read.

L.1 MIXTURE OF GOOD AND BAD SAMPLES (CIFAR-10)

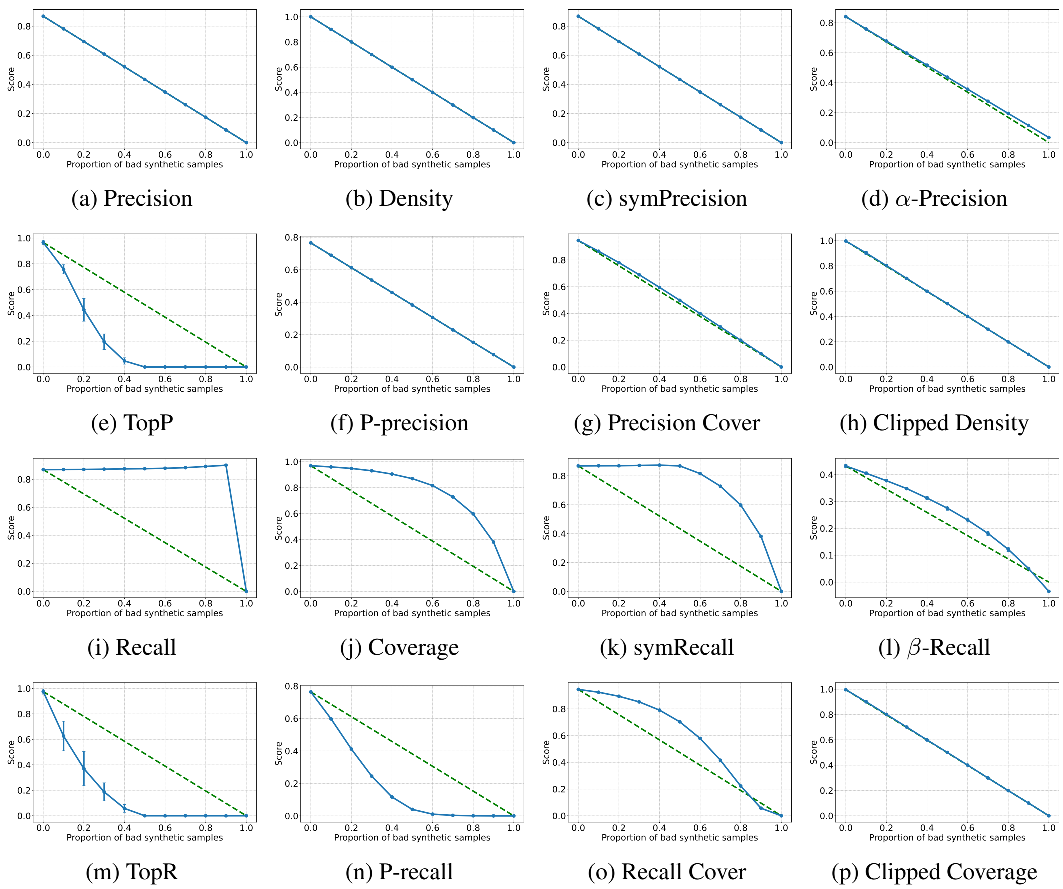

(a) Precision (b) Density (c) symPrecision (d) α-Precision

(e) TopP (f) P-precision (g) Precision Cover (h) Clipped Density

(i) Recall (j) Coverage (k) symRecall (l) β-Recall

(m) TopR (n) P-recall (o) Recall Cover (p) Clipped Coverage

Figure 17: **Mixture of good and bad samples (CIFAR-10), unnormalized.**

L.2 SIMULTANEOUS MODE DROPPING (CIFAR-10)

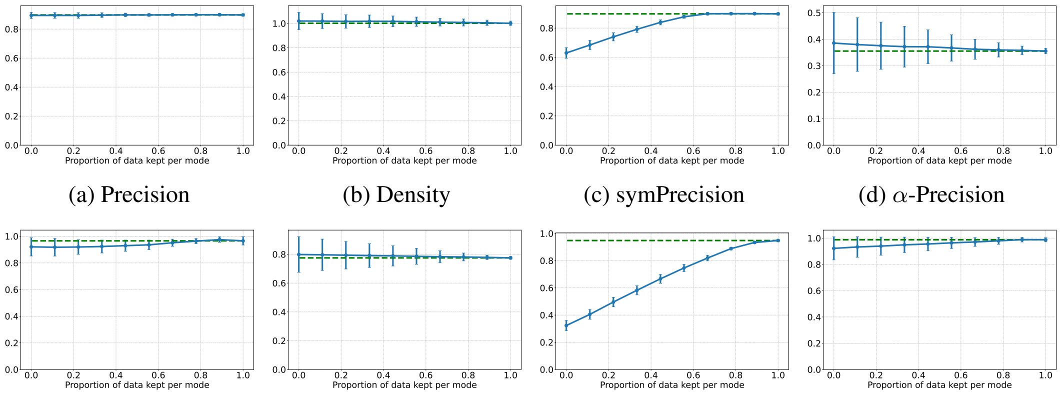

(a) Precision (b) Density (c) symPrecision (d) α-Precision

(e) TopP (f) P-precision (g) Precision Cover (h) Clipped Density

Figure 18: **Simultaneously dropping modes (CIFAR-10), unnormalized.**

L.3 MATCHED REAL & SYNTHETIC OUT-OF-DISTRIBUTION SAMPLES (CIFAR-10)

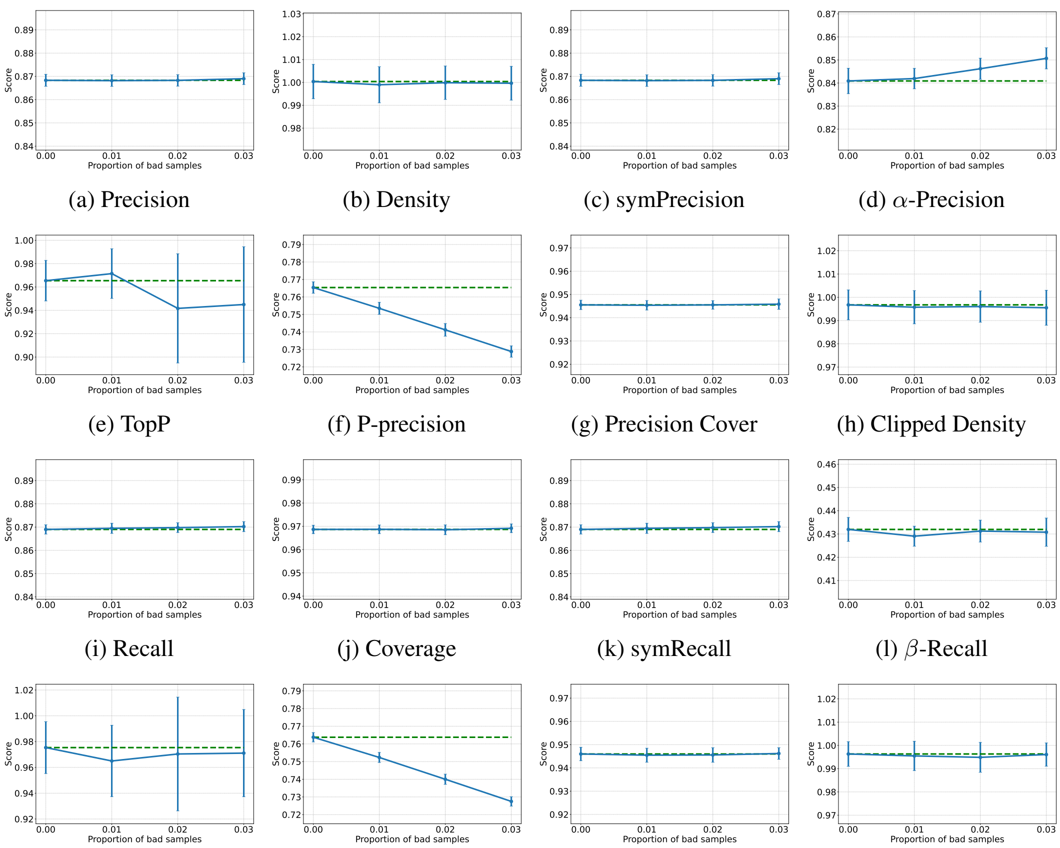

(a) Precision (b) Density (c) symPrecision (d) α-Precision

(e) TopP (f) P-precision (g) Precision Cover (h) Clipped Density

(i) Recall (j) Coverage (k) symRecall (l) β-Recall

(m) TopR (n) P-recall (o) Recall Cover (p) Clipped Coverage

Figure 19: **Matched real & synthetic out-of-distribution samples (CIFAR-10), unnormalized.**

L.4 Synthetic distribution translation

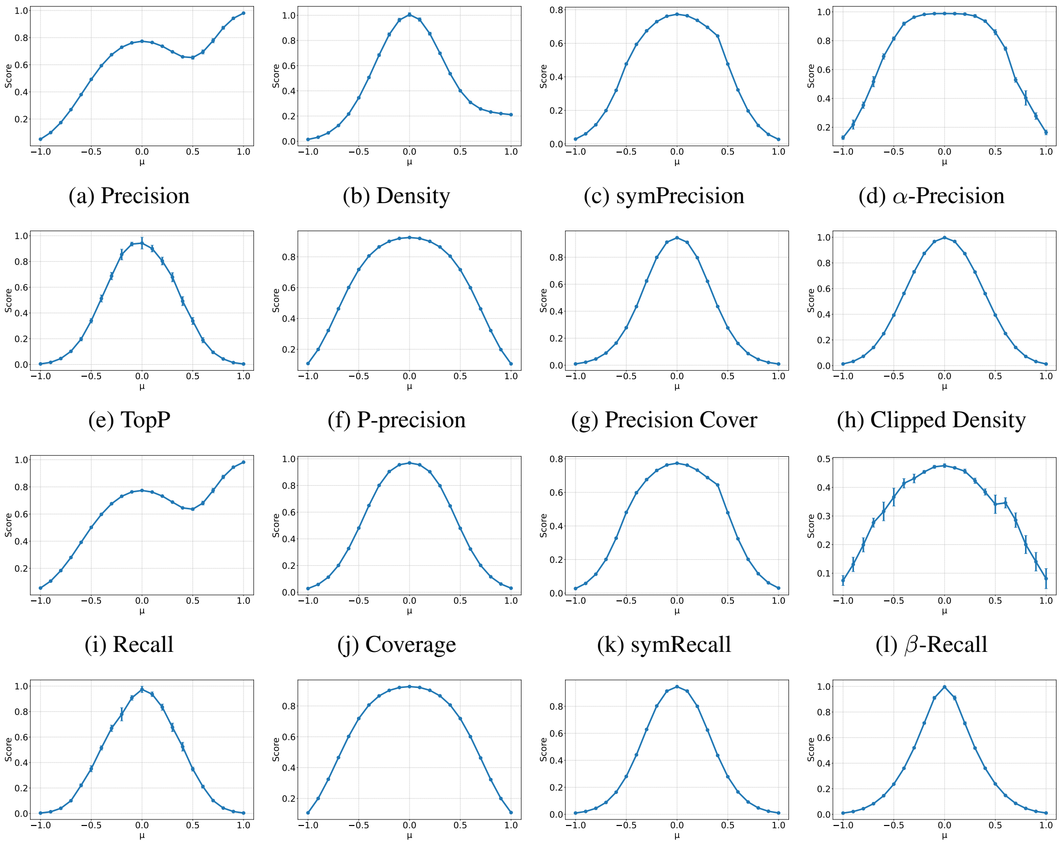

(a) Precision (b) Density (c) symPrecision (d) α-Precision

(e) TopP (f) P-precision (g) Precision Cover (h) Clipped Density

(i) Recall (j) Coverage (k) symRecall (l) β-Recall

(m) TopR (n) P-recall (o) Recall Cover (p) Clipped Coverage

Figure 20: **Translating a synthetic Gaussian with 2 bad samples, unnormalized.**